TLC showed that there was some reduction product, but a great deal of total decomposition was obvious. Workup as above gave a small quantity of reduction product which was not sufficient for characterization. Reduction of $CH_3CD_2C(O)CCo_3(CO)_9$ (1.0 mmol) with 1.5 mL of $CF_3CO_2H$ in 50 mL of benzene at reflux (4-h reaction time), on the other hand, was successful. Workup as above gave 0.11 g (23%) *n*-butylidynetricobalt nonacarbonyl which NMR showed to be a mixture of the various combinations of $\alpha$- and $\beta$-deuterated compounds.

**Reduction of (Isopropenylmethylidyne)tricobalt Nonacarbonyl with Deuteriotrifluoroacetic Acid.** The usual apparatus was charged with 0.48 g (1.0 mmol) of $CH_2{=}CMeCCo_3(CO)_9$,[27] 2 mL of $CF_3CO_2D$, and 50 mL of benzene. After this solution had been stirred and heated at reflux under nitrogen for 4 h, removal of volatiles and column chromatography of the residue gave 0.25 g (52%) of (2-methylpropylidyne)tricobalt nonacarbonyl which had an IR spectrum identical with that of an authentic sample. The proton NMR spectrum suggested that it was a mixture of the following deuterated compounds: $CH_3(CH_2D)CDCCo_3(CO)_9$, $CH_3(CHD_2)CHCCo_3(CO)_9$, and $(CH_2D)_2CHCCo_3(CO)_9$. NMR ($CDCl_3$): $\delta$ 1.35-1.7 (m, ca. 4.4 H, $CH_3$), 3.6-4.0 (m, 1 H, $CHMe_2$). The proton NMR spectrum did not match that expected for any one of the above products but appeared to represent a combination of the various deuterated products.

**Reduction of (Propanoylmethylidyne)tricobalt Nonacarbonyl with Acetic Acid.** The standard apparatus used in the $CF_3CO_2H$ reductions was charged with 0.5 g (1.0 mmol) of $C_2H_5C(O)CCo_3(CO)_9$, 1.5 mL of glacial acetic acid, and 50 mL of benzene. The mixture was stirred and heated at reflux under nitrogen. After 2 h, TLC showed that all of the starting ketone had been consumed and that two products, one of higher and the other of lower $R_f$ than the ketone, were present. The usual workup gave 0.03 g (6%) of $n$-$C_3H_7CCo_3(CO)_9$ and 0.29 g (58%) of $C_2H_5CH(OH)CCo_3(CO)_9$, mp 136-138 °C (lit.[6] mp 137-138 °C). Both products were identified by comparison of their IR spectra with those of authentic samples.

A similar reaction with 1.0 mmol of $Me_2CHC(O)CCo_3(CO)_9$ with 1 mL of glacial acetic acid in refluxing benzene solution for 5 h gave a very small quantity of $Me_2CHCH_2CCo_3(CO)_9$ and 0.21 g (41%) of $Me_2CHCH(OH)CCo_3(CO)_9$, mp 113-115 °C (lit.[6] mp 114-116 °C).

**Dehydrogenation of (2-Hydroxyalkylidyne)tricobalt Nonacarbonyl Complexes in Refluxing Benzene.** The example of (2-hydroxy-3-methylbutylidyne)tricobalt nonacarbonyl is typical.

A 100-mL three-necked flask equipped with a magnetic stir bar and a reflux condenser topped with a nitrogen inlet tube was purged with nitrogen and charged with 1.03 g (2.0 mmol) of $Me_2CHCH(OH)CCo_3(CO)_9$ and 50 mL of benzene. The solution was stirred and heated at reflux under nitrogen for 4 h, until TLC showed the absence of starting material and the presence of two products which gave purple and brown spots, respectively. Both were of higher $R_f$ than the starting alcohol. The solvent was removed under reduced pressure, and the residue was purified by column chromatography to yield 0.10 g (10%) of $Me_2CHCCo_3(CO)_9$ and 0.54 g (53%) of $Me_2CHC(O)CCo_3(CO)_9$, mp 150-153 °C (lit.[3] mp 150-153 °C dec). Both compounds were identified by comparison of their IR spectra with those of authentic samples.

This reaction was repeated by using 0.40 g (0.78 mmol) of the alcohol in 50 mL of benzene, but 10 drops of alcoholic sodium hydroxide also were added. A 2.5-h reflux period sufficed to consume the starting material. TLC showed that a single product (brown spot) of higher $R_f$ had been formed. Workup as above gave 0.28 g (70%) of $Me_2CHC(O)CCo_3(CO)_9$, mp 151-153 °C.

In the case of $ArCH(OH)CCo_3(CO)_9$ compounds only the decarbonylation products were obtained. When 0.55 g (1.0 mmol) of $PhCH(OH)CCo_3(CO)_9$ in 50 mL of benzene was heated at reflux under nitrogen, TLC (1:3 $CH_2Cl_2$/hexane) indicated that the ketone was forming but that it was decarbonylating as it was being formed. After 6 h at reflux, no starting alcohol remained. Removal of solvent was followed by column chromatography of the residue to give 0.28 g (54%) of $PhCCo_3(CO)_9$ (mp 105-106 °C), identified by comparison of its IR spectrum with that of an authentic sample.

**Acknowledgment.** The authors are grateful to the National Science Foundation for support of this work.

(27) Seyferth, D.; Eschbach, C. S.; Williams, G. H.; Hung, P. L. K. *J. Organomet. Chem.* **1977**, *134*, 67.

# Metalloporphyrins with Unusual Geometries. 1. Mono-, Di-, Triatom-Bridged Porphyrin Dimers

**Kazuyuki Tatsumi and Roald Hoffmann***

*Contribution from the Department of Chemistry, Cornell University, Ithaca, New York 14853.*
*Received September 24, 1980*

**Abstract:** The electronic structure of mono-, di-, and triatom-bridged metalloporphyrin dimers is examined to show how orbital symmetries and electron counts determine their geometries and electronic properties. An orbital diagram constructed for $(N_4M)$—X—$(MN_4)$, where $N_4$ is a model porphyrin and X denotes an O, N, or C atom, accounts for the bending preference and magnetic behavior of the X = O, N species. The analysis of the diagram leads us to predict that the carbido-bridged complexes should be stable diamagnetic molecules having a linear M—C—M spine. The Walsh diagram for bending of the M—O—O bonds in $(N_4M)$—O—O—$(MN_4)$ shows that geometrical preferences of M = Fe and M = Co compounds are very much alike. Although the normal trans bent M—O—O—M structure is calculated to be most stable, a cis bent alternative is also a possibility, if the steric constraints allow it. A side-on structure, which may be accessible for low d-electron counts, is at relatively high energy for $d^4$-$d^4$ metals. The simultaneous 1,2 migration of two metalloporphyrin fragments on $O_2$ encounters a level crossing between occupied and unoccupied valence orbitals for M = Co and Fe. Two remarkably different molecular structures of an $M_2O_3^{4+}$ unit in (O═Mo—porphyrin)—O—(porphyrin—Mo═O) and (Nb—porphyrin)—$O_3$—(Nb—porphyrin) can be explained by optimal M—O $\pi$ interactions.

Metalloporphyrins in protein systems perform an important class of biochemical functions in nature. Hemoglobin, myoglobin, chlorophyll, cytochromes, catalase, and peroxidase are all well-known examples, the chemistry of which relates principally to redox reactions and the transport, storage, and activation of molecular oxygen. Over the years a great biochemical effort has brought us substantial understanding of the structure-function relationship in these natural metalloporphyrins.

Inorganic chemists have been very active in this field as well. They have made a large number of synthetic models for naturally occurring metalloporphyrins in their effort to determine the factors which govern the biological function of the natural porphyrins

0002-7863/81/1503-3328$01.25/0 

and to mimic their biological efficiency in vitro.[1] Although nature has outdone chemists in creating compounds suited for specific tasks, "model porphyrins" have unfolded a rich and beautiful chemistry of their own. The simplest and most frequently encountered class of synthetic porphyrins is the monometallic single-porphyrin type where, in many cases, a central metal takes up an additional one or two donor ligands to complete its coordination sphere (see **1**). Various synthetic metalloporphyrins and

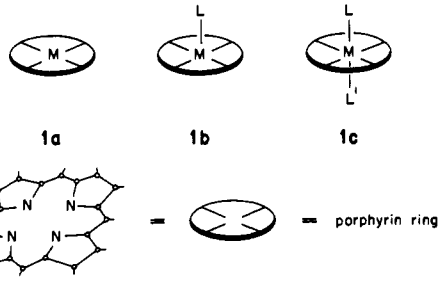


their dioxygen adducts are extensively studied examples of this type, which frequently incorporate an ingeniously modified porphyrin ring.[2] It is no accident that much theoretical effort has been directed to this particular area.[3]

Besides this class, the prosperity of synthetic porphyrin chemistry has provided metalloporphyrins with more unusual geometries.[4] Some of these are mono-, di-, triatom-bridged porphyrin dimers (M–porphyrin)$_2$X, X = O, N, $O_2$, and $O_3$, skewed out-of-plane metalloporphyrins $(ML_n)_2$(porphyrin), M = Tc, Rh, Re, and carbene-inserted metalloporphyrins Ni($N_4$–TPP)–CHR etc. What causes the variegated geometries, which often accompany unique electronic and magnetic properties? In this paper, part 1 of our theoretical study of these geometrically unusual metalloporphyrins, we will focus our attention on mono-, di-, triatom-bridged porphyrin dimers. Our purpose is to show how symmetry-imposed restrictions rationalize their unusual geometries and to determine what kind of metal or what number of d electrons can create these geometries. The theoretical analyses are based on the extended Hückel method, with parameters specified in the Appendix.

**Reduced Porphyrin and Its Model $(NH_2)_4^{4-}$.** The first theoretical analysis of porphyrins dates back to the pioneering work by Longuet-Higgins, Rector, and Platt,[5] which was followed by Kobayashi's PPP-type calculations[6] and an extensive and elegant series of studies by the Gouterman group.[7] More recently ab initio[8] and MSW-X$\alpha$ methods[9] have been applied to this area. Thus a great deal is known about the electronic structure of porphyrins and metalloporphyrins.

The porphyrin dianion **2** consists of four pyrrole-type rings

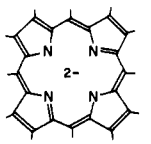


**2**

joined by four methine bridges to give a planar $N_4$ macrocycle. The highly conjugated system is the origin of the strong color of

(1) Recently published reviews on metalloporphyrins: (a) Buchler, J. W.; Kokisch, W.; Smith, P. D. *Struct. Bonding (Berlin)* **1978**, *34*, 79–134. (b) Dolphin, D.; Addison, A. W.; Cairns, M.; Dinello, R. K.; Farrell, N. P.; James, B. R.; Paulson, D. R.; Welborn, C. *Int. J. Quantum Chem.* **1979**, *16*, 311–329. (c) Dilworth, J. R.; Leigh, G. J.; Richards, R. L.; Bagnall, K. W. *Annu. Rep. Prog. Chem., Sect. A: Phys. Org. Chem.* **1978**, *74*, 169–214. (d) Dolphin, D., Ed. "The Porphyrins"; Academic Press: New York, 1978, 1979; Vol. I–VII. (e) Suckling, C. J.; Suckling, K. E.; Suckling, C. W. "Chemistry Through Models"; Cambridge University Press: Cambridge, 1977: pp 217–225. (f) Cohen, I. A. *Structure Bonding (Berlin)* **1980**, *40*, 1–37.

(2) (a) For recent reviews see the following: Basolo, F.; Hoffman, B. M.; Ibers, J. A. *Acc. Chem. Res.* **1975**, *8*, 384–392. Fuhrhop, J. H. *Angew. Chem., Int. Ed. Engl.* **1976**, *15*, 648–659. Collman, J. P. *Acc. Chem. Res.* **1977**, *10*, 265–272. Jones, R. D.; Summerville, D. A.; Basolo, F. *Chem. Rev.* **1979**, *79*, 139–179. (b) Collman, J. P.; Gagne, R. R.; Reed, C. A.; Robinson, W. T.; Rudley, G. A. *Proc. Natl. Acad. Sci. U.S.A.* **1974**, *71*, 1326–1329. Collman, J. P.; Reed, C. A. *J. Am. Chem. Soc.* **1973**, *95*, 2048–2049. Collman, J. P.; Gagne, R. R.; Halbert, T. R.; Marchon, J.-C.; Reed, C. A. *Ibid.* **1973**, *95*, 7868–7870. Collman, J. P.; Gagne, R. R.; Reed, C. A.; Halbert, T. R.; Land, G.; Robinson, W. T. *Ibid.* **1975**, *97*, 1427–1439. Collman, J. P.; Brauman, J. I.; Halbert, T. R.; Suslick, K. S. *Proc. Natl. Acad. Sci. U.S.A.* **1976**, *73*, 3333–3337. Jameson, G. B.; Molinaro, F. S.; Ibers, J. A.; Collman, J. P.; Brauman, J. L.; Rose, E.; Suslick, K. S. *J. Am. Chem. Soc.* **1980**, *102*, 3224–3237. (c) Almog, J.; Baldwin, J. E.; Dyer, R. L.; Peters, M. *Ibid.* **1975**, *97*, 227–228. Baldwin, J. E.; Huff, J. *Ibid.* **1973**, *95*, 5757–5759. Baldwin, J. E.; Klose, T.; Peters, M. *J. Chem. Soc., Chem. Commun.* **1976**, 881–883. Baldwin, J. E.; Debernardis, J. F. *J. Org. Chem.* **1977**, *42*, 3986–3987. Budge, J. R.; Ellis, P. F., Jr.; Jones, R. D.; Linard, J. E.; Basolo, F.; Baldwin, J. E.; Dyer, R. L. *J. Am. Chem. Soc.* **1979**, *101*, 4761–4762. Budge, J. R.; Ellis, P. E., Jr.; Jones, R. D.; Linard, J. E.; Szymanski, T.; Basolo, F.; Baldwin, J. E.; Dyer, R. L. *Ibid.* **1979**, *101*, 4762–4763. (d) Chang, C. K.; Traylor, T. G. *Proc. Natl. Acad. Soc. U.S.A.* **1973**, *70*, 2647–2650; *Ibid.* **1975**, *72*, 1166–1170. *J. Am. Chem. Soc.* **1973**, *95*, 5810–5811, 8477–8479. Bringer, W. S.; Chang, C. K. *Ibid.* **1974**, *96*, 5595–5597. Bringer, W. S.; Chang, C. K.; Geibel, J.; Traylor, T. G. *Ibid.* **1974**, *96*, 5597–5599. Geibel, J.; Chang, C. K.; Traylor, T. G. *Ibid.* **1975**, *97*, 5924–5926. Geibel, J.; Cannon, J.; Campbell, D.; Traylor, T. G. *Ibid.* **1978**, *100*, 3575–3585. (e) Vaska, L.; Amundsen, A. R.; Brady, R.; Flynn, B. R.; Nakai, H. *Finn. Chem. Lett.* **1974**, *2*, 66–69. Amundsen, A. R.; Vaska, L. *Inorg. Chim. Acta* **1975**, *14*, L49–L51. (f) Weschler, C. J.; Hoffman, B. M.; Basolo, F. *J. Am. Chem. Soc.* **1975**, *97*, 5278–5280. Hoffman, B. M.; Weschler, C. J.; Basolo, F. *Ibid.* **1976**, *98*, 5473–5482. Hoffman, B. M.; Szymanski, T.; Brown, T. G.; Basolo, F. *Ibid.* **1978**, *100*, 7253–7259. Jones, R. D.; Summerville, D. A.; Basolo, F. *Ibid.* **1978**, *100*, 4416–4424. (g) Latour, J.-M.; Marchon, J.-C.; Nakajima, M. *Ibid.* **1979**, *101*, 3974–3976. (h) James, B. R.; Stynes, D. V. *Ibid.* **1972**, *94*, 6225–6226. Stynes, D. V.; Stynes, H. C.; Ibers, J. A.; James, B. R. *Ibid.* **1973**, *95*, 1142–1149 and references therein. (i) Walker, F. A. *Ibid.* **1970**, *92*, 4235–4244; **1973**, *95*, 1154–1159. (j) Wayland, B. B.; Minikiewicz, J. V.; Add-Elmageed, M. E. *Ibid.* **1974**, *96*, 2795–2801. (k) Cheung, S. K.; Grimes, C. J.; Wong, J.; Reed, C. A. *Ibid.* **1976**, *98*, 5028–5030. (l) Guilard, R.; Fournari, M.; Lecomte, C.; Protas, J. *J. Chem. Soc., Chem. Commun.* **1976**, 161–162. (m) Chevrier, B.; Diebolo, Th.; Weiss, R. *Inorg. Chim. Acta* **1976**, *19*, L57–L58. (n) Drago, R. J.; Bevgelsdijk, T.; Breese, J. A.; Cannady, J. P. *J. Am. Chem. Soc.* **1978**, *100*, 5374–5382. (o) Inner-sphere and outer-sphere dioxygen complexes as intermediate of autoxidation reactions, see: Billecke, J.; Kokisch, W.; Buchler, J. W. *J. Am. Chem. Soc.* **1980**, *102*, 3622–3624 and references therein.

(3) (a) Pauling, L.; Coryell, C. D. *Proc. Natl. Acad. Sci. U.S.A.* **1936**, *22*, 210–216. Pauling, L. *Ibid.* **1977**, *74*, 2612–2613. (b) Seno, Y.; Otsuka, J.; Matsuoka, O.; Fuchikami, N. *J. Phys. Soc. Jpn.* **1972**, *33*, 1645–1660. Otsuka, J.; Matsuoka, O.; Fuchikami, N.; Seno, Y. *Ibid.* **1973**, *35*, 854–860. Seno, Y.; Kameda, N.; Otsuka, J. *J. Chem. Phys.* **1980**, 6048–6058, 6059–6069. (c) Rohmer, M.-M.; Dedieu, A.; Veillard, A. *Theor. Chim. Acta* **1975**, *39*, 189–195. Dedieu, A.; Rohmer, M.-M.; Benard, M.; Veillard, A. *J. Am. Chem. Soc.* **1976**, *98*, 3717–3718. Dedieu, A.; Rohmer, M.-M.; Veillard, A. *Ibid.* **1976**, *98*, 5789–5800; *Bull. Soc. Chim. Belg.* **1976**, *85*, 953–962. Dedieu, A.; Rohmer, M.-M. *J. Am. Chem. Soc.* **1977**, *99*, 8050–8051. (d) Loew, G. H.; Kirchner, R. F. *Ibid.* **1975**, *97*, 7388–7390. Kirchner, R. F.; Loew, G. H. *Ibid.* **1977**, *99*, 4639–4647. Loew, G. H.; Kirchner, R. F. *Int. J. Quantum Chem. Quantum Biol. Symp.* **1978**. Herman, Z. S.; Loew, G. H. *J. Am. Chem. Soc.* **1980**, *102*, 1815–1821. (e) Goddard, W. A., III; Olafson, B. D. *Proc. Natl. Acad. Sci. U.S.A.* **1975**, *72*, 2335–2339. (f) Eaton, W. A.; Hanson, L. K.; Stephens, P. J.; Sutherland, J. C.; Dunn, J. B. R. *J. Am. Chem. Soc.* **1978**, *100*, 4991–5003. (g) Huynh, B. H.; Case, D. A.; Karplus, M. *Ibid.* **1977**, *99*, 6103–6105. Case, D. A.; Huynh, B. H.; Karplus, M. *Ibid.* **1979**, *101*, 4433–4453. (h) Makinen, M. W.; Churg, A. K.; Glick, H. A. *Proc. Natl. Acad. Sci. U.S.A.* **1978**, *75*, 2291–2295. (i) Cox, G. S.; Whitten, D. G.; Giannotti, C. *Chem. Phys. Lett.* **1979**, *67*, 511–515. (j) Hanson, L. K.; Hoffman, B. M. *J. Am. Chem. Soc.* **1980**, *102*, 4602–4609.

(4) Reviews: (a) Tsutsui, M.; Taylor, G. A. "Porphyrins and Metalloporphyrins"; Smith, K. M., Ed.; Elsevier: Amsterdam, 1975; pp 279–313. (b) Buchler, J. W. *Ibid.*, pp 157–231; "The Porphyrins"; Dolphin, D. E., Academic Press: New York, 1978; Vol. I, pp 389–483.

(5) Longuet-Higgins, H. C.; Rector, C. W.; Platt, J. R. *J. Chem. Phys.*, **1950**, *18*, 1174–1181.

(6) Kobayashi, H. *J. Chem. Phys.* **1959**, *30*, 1362–1363, 1373–1374.

(7) Gouterman, M. *J. Mol. Spectrosc.* **1961**, *6*, 138–163. Gouterman, M.; Wagniere, G. H. *Ibid.* **1963**, *11*, 108–127. Weiss, C., Jr.; Kobayashi, H.; Gouterman, M. *Ibid.* **1965**, *16*, 415–450. Zerner, M.; Gouterman, M. *Theoret. Chim. Acta* **1966**, *4*, 44–63; *Inorg. Chem.* **1966**, *5*, 1699–1706, 1707–1709. Zerner, M.; Gouterman, M.; Kobayashi, H. *Theor. Chim. Acta* **1966**, *6*, 363–400; Zerner, M.; Gouterman, M. *Ibid.* **1967**, *8*, 26–34. Ake, R. L.; Gouterman, M. *Ibid.* **1970**, *17*, 408–416. Schaffer, A. M.; Gouterman, M. *Ibid.* **1970**, *18*, 1–13; **1972**, *25*, 62–82. McHugh, A. J.; Gouterman, M. *Ibid.* **1972**, *24*, 346–370. Schaffer, A. M.; Gouterman, M.; Davidson, E. R. *Ibid.* **1973**, *30*, 9–30. Antipas, A.; Buchler, J. W.; Gouterman, M.; Smith, P. D. *J. Am. Chem. Soc.* **1978**, *100*, 3015–3024. Antipas, A.; Dolphin, D.; Gouterman, M.; Johnson, E. C. *Ibid.* **1978**, *100*, 7705–7709. Spellane, P. J.; Gouterman, M.; Antipas, A.; Kim, S.; Liu, Y. C. *Inorg. Chem.* **1980**, *19*, 386–391.

(8) (a) see ref 3c. (b) Spangler, D.; Maggiora, G. M.; Shipman, L. L.; Christofferson, R. E. *J. Am. Chem. Soc.* **1977**, *99*, 7470–7477, 7478–7489.

(9) (a) see ref 3g. (b) Case, D. A.; Karplus, M. *J. Am. Chem. Soc.* **1977**, *99*, 6182–6194.

porphyrin compounds and plays an important role in their oxidation–reduction properties. The porphyrin dianion also provides a vacant site at its center, ideally prepared for metal incorporation. The tetradentate ligand completes well a square-planar, square-pyramidal, or octahedral coordination environment, and it contains sufficient space to accommodate most any metal and has built into it some conformational flexibility to accommodate metal ions of larger radius.

The essence of bonding between a central metal atom and this tetradentate ligand is to be found in the following two types of primary interactions—$\sigma$ coordination of nitrogen lone pairs directed toward the center of the ring and $\pi$ interaction of metal $p_\pi$ and/or $d_\pi$ with nitrogen $p_\pi$ orbitals.[10] The symmetry aspects of these interactions are familiar—the appropriate symmetry-adapted linear combinations of ligand orbitals are shown schematically in **3**. The central metal atom bonds to the tetradentate

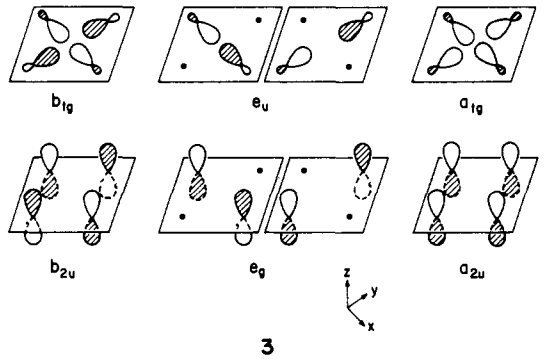


**3**

ligand surrounding it through interactions of $d_{x^2-y^2}$–$b_{1g}$, $d_{xz}$ and $d_{yz}$–$e_g$, $d_{z^2}$ and s–$a_{1g}$, $p_x$ and $p_y$–$e_u$, and $p_z$–$a_{2u}$ pairs. Each interaction may be spread out over several orbitals in the porphyrin system—this is just a summary of the symmetry types. In the $\sigma$ system the porphyrin is clearly a donor to the metal. What about the $\pi$ system? Clearly the porphyrin has the appropriate orbitals to act both as a $\pi$ donor and as an acceptor. But the calculations indicate that it is on the donor side—for instance the N $2p_z$ orbital is occupied by a net 1.61 electrons in a free porphyrin dianion.

The metalloporphyrin complexes of interest to us are quite large molecules. One basic porphyrin dianion unit has 108 valence orbitals, and we wanted to treat molecules containing two such units, two metal atoms, and for good measure several other ligands as well—often in a situation of low symmetry. Reasons of computational economy thus forced us to examine a simplification of the porphyrin ring. Our guide in this simplification was the realization that our interest resides in ground-state properties of the metalloporphyrins and not in their (important) excited states. For this specific purpose, the large conjugated system of the porphyrin may not be crucial. If a model porphyrin contains the orbital set delineated in **3**, perhaps it is sufficient to describe the bonding in even larger, composite metalloporphyrins. Considering thus the minimal requirements for a model porphyrin, we simplified the ring progressively from **2** to **4** and finally to **6**,

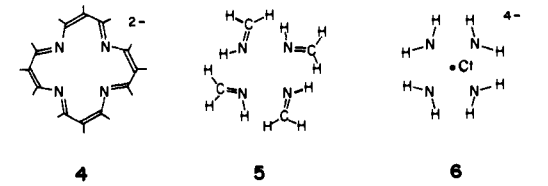


**4** **5** **6**

$(NH_2^-)_4$. **4** was still too large for our purposes, and **5** failed to retain the $D_{4h}$ symmetry which so facilitated the theoretical analysis. In the tetraamido model **6**, four nitrogens of the model ligand provide properly a set of lone-pair orbitals and four doubly occupied $p_\pi$ orbitals shown above in **3**. In the $D_{4h}$ arrangement of $(NH_2)_4^{4-}$ the H–N–H angle of 106.4° and a distance between

(10) Minor interactions between a central metal and the porphyrin ring arise from combinations of N pseudo-$\pi$ orbitals and metal orbitals: $e_u$-$(N_4)$–$p_xp_y$(M), $b_{2g}$–$d_{xy}$. The $a_{2g}$ combination of N pseudo-$\pi$ finds no metal orbitals with which to interact.

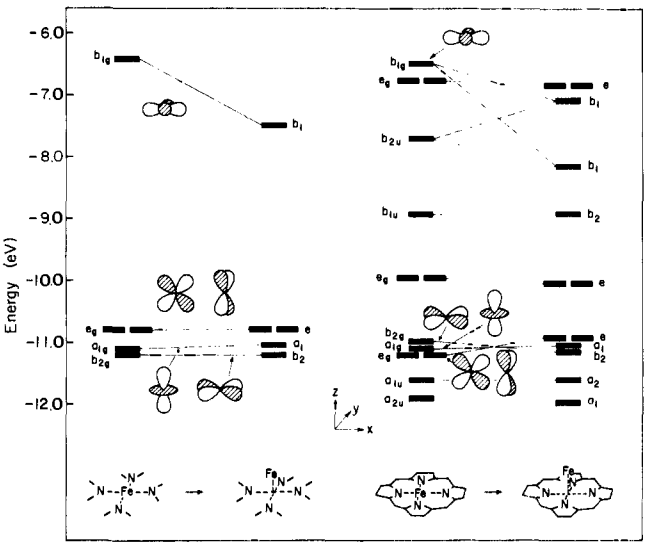


**Figure 1.** Levels of Fe(porphyrin) and its model compound $Fe(NH_2)_4^{2-}$. The right half of the figure shows the levels of Fe(porphyrin) and the left half shows those of $Fe(NH_2)_4^{2-}$. From left to right in each half: the Fe atom sits in the middle of the porphyrin or $(NH_2)_4$ plane; Fe moves up by 0.5 Å out of the plane.

the center Ct and N atom (2.027 Å) were taken from the corresponding C–N–C angle and Ct–N distance in Fe(TPP)–O–Fe(TPP).[11a] The N–H distance is assumed to be 1.02 Å. We abbreviate this model as "$N_4$" throughout this paper.

The metalloporphyrins which we examine in our work contain M(porphyrin) "fragments" where a metal M is either in the middle of the porphyrin plane or out of that plane. Exploratory calculations were then carried out for in- and out-of-phase geometries of the fragment $Fe^{II}$(porphyrin) and its model $Fe^{II}(N_4)^{2-}$ to see how our simplest model preserves the orbital pattern of $Fe^{II}$-(porphyrin). The valence orbitals are shown in Figure 1. For *both* $Fe^{II}$(porphyrin) and $Fe^{II}(N_4)^{2-}$ in a $D_{4h}$ square-planar geometry, the four lower d orbitals, $xy$ ($b_{2g}$), $z^2$ ($a_{1g}$), and a degenerate pair $xz$, $yz$ ($e_g$), are located very close to each other in energy. No wonder that the order of d orbitals is very sensitive to a small change in geometrical parameters of the porphyrin and to a calculational method chosen.[3,5-9] In our calculations $xy > z^2 > xz, yz$ for $Fe^{II}$(porphyrin) and $xz, yz > z^2 > xy$ for $Fe^{II}(N_4)^{2-}$. A small out-of-plane displacement of Fe(II) affects these orbitals, but not significantly, for both $Fe^{II}$(porphyrin) and $Fe^{II}(N_4)^{2-}$ retain the lower d block with the order $xz, yz > z^2 > xy$. Other orbitals of $Fe^{II}$(porphyrin) in Figure 1 consist primarily of $Cp_\pi$ orbitals of a porphyrin and are nearly innocent of metal–porphyrin interaction. Perhaps the major weakness of the model is the absence in it of any acceptor characteristic of the porphyrin ring. Thus the model lacks the counterpart of the two higher lying $e_g$ sets of the porphyrin. Being aware of this shortcoming we returned to the full porphyrin for checks in our subsequent work, whenever we perceived that porphyrin-acceptor properties were of possible importance.

**Single-Atom-Bridged Porphyrin Dimers.**[12] Two metalloporphyrins may be linked at the metal through a single atom X (see **7**). Such $\mu$-oxo-porphyrin dimers have often been reported,

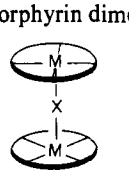


**7**

(11) (a) Hoffman, A. B.; Collins, D. M.; Day, V. W.; Fleischer, E. B.; Srivastava, T. S.; Hoard, J. L. *J. Am. Chem. Soc.* **1972**, *94*, 3620–3626. (b) Fleischer, E. B.; Srivastava, T. S. *Ibid.* **1969**, *91*, 2403–2405. (c) Cohen, I. A. *Ibid.* **1969**, *91*, 1980–1983.

(12) A short communication of this section has been published: Tatsumi, K.; Hoffmann, R.; Whangbo, M.-H. *J. Chem. Soc., Chem. Commun.* **1980**, 509–511.

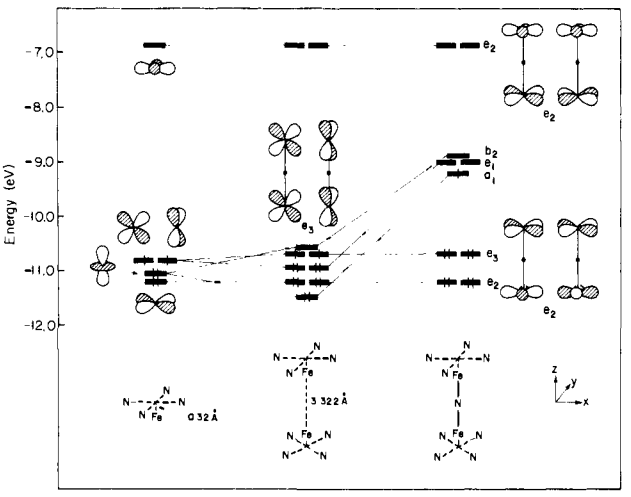


**Figure 2.** The building up of the orbitals of $N_4Fe-N-FeN_4$. From left to right: the orbitals of the pyramidal $N_4Fe$ in which Fe is displaced by 0.32 Å out of the $N_4$ plane; two such pyramidal $N_4Fe$ units brought to 3.322 Å separation between the irons, the orbitals of the composite nitrido complex. The electron count shown is that appropriate to a low-spin Fe-N-Fe complex.

while X-ray diffraction analyses are available for (Fe—TPP)$_2$O[11] and (O=Mo—TPP)$_2$O.[13] Also we have plenty of structural data for equivalent $\mu$-oxo dimers which contain Schiff bases[14] or phthalocyanines (Pc) instead of porphyrin rings.[15] For X = N we have, so far, a single example.[16] While severely constrained by the steric bulk of the macrocyclic ligands, these bridged molecules nevertheless exhibit a range of bending angle at X. The smallest angle, 139°, was observed for (Fe—salen)$_2$O·(py)$_2$[17] (**8a**),

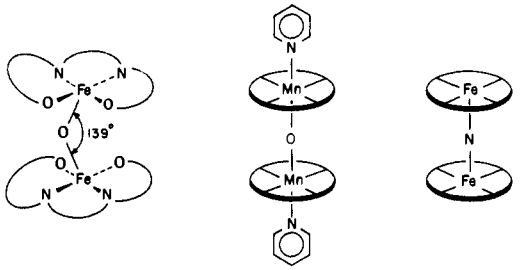


**8a** **8b** **8c**

the largest, linearity, being typified by (py—Mn—Pc)$_2$O[15] (**8b**) and (Fe—TPP)$_2$N (**8c**). Another interesting feature of these bridged dimers is the remarkable range of their magnetic properties. The bridging atom can support strong electronic interactions between the two metal sites so that chemical and physical properties of the dimer may differ substantially from related monomers.

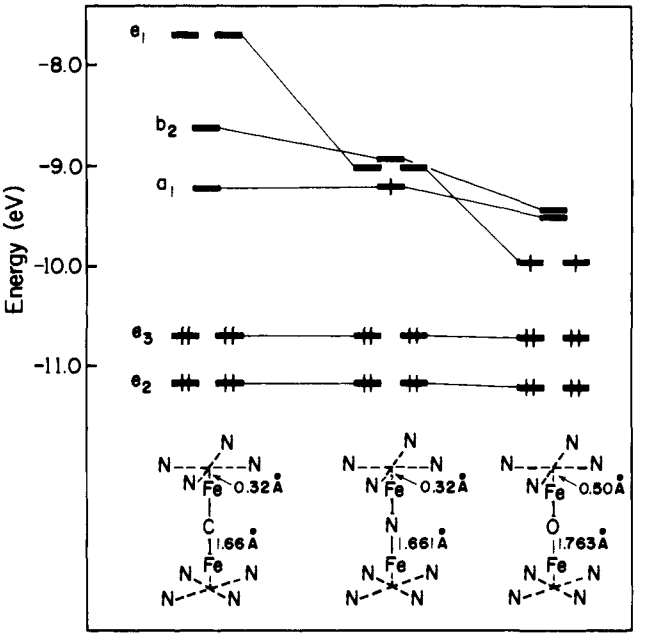


**Figure 3.** The valence orbitals of $N_4Fe-X-FeN_4$ for X = C, N, and O. The electron count shown is for a low-spin Fe-X-Fe configuration.

The construction of the molecular orbitals for $(Fe-N_4)_2X$ is illustrated by nitrido-bridged dimers (X = N) in Figure 2. The iron atom is displaced by 0.32 Å out of the $N_4$ plane, while the Fe-bridging N distance is taken as 1.661 Å. The symmetry is $D_{4d}$, staggered $N_4$ units. These geometrical parameters are derived from the data of the X-ray diffraction analysis of (Fe-TPP)$_2$N.[16a]

The theoretical analysis follows familiar lines.[18] The first column of Figure 2 shows the d orbital splitting of the pyramidalized Fe($N_4$), in which a nest of four d orbitals is far below the high-lying $x^2-y^2$ orbital. The pyramidal Fe($N_4$) units are brought to 3.322 Å of each other in the second column. The direct through-space overlap of these orbitals is not great, leading to the small splitting. The orbitals are still easily recognized as in- and out-of-phase combinations of $xy$, $x^2-y^2$ ($e_2$), $z^2$ ($a_1$ and $b_2$), and $xz$, $yz$ ($e_1 + e_3$). Now the interaction with the bridging atom N is introduced. N bears orbitals of $a_1$ (2s) and $b_2 + e_1$ (2p) symmetry. In the high $D_{4d}$ symmetry the $e_2$ and $e_3$ d block combinations are left alone, and the $a_1$, $b_2$, and $e_1$ molecular orbitals mix to a varying degree with N orbitals (see 9). These orbitals

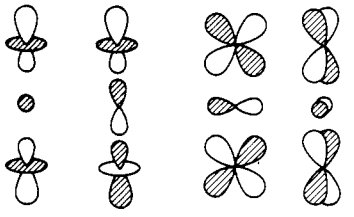


**9**

are destabilized according to the strength of the Fe-bridging atom antibonding interaction.

For a bridging N, the four levels are very nearly degenerate in our calculations. Then the odd electron of (Fe-TPP)$_2$N may sit in either of these levels. The other eight electrons in Figure 2 reside in four low-lying $e_2$ and $e_3$ orbitals which are well separated in energy from the four destabilized levels. We expect the ground state of (Fe-TPP)$_2$N to be a low-spin doublet. The very

(13) (a) Fleischer, E. B.; Srivastava, T. S. *Inorg. Chim. Acta* **1971**, *5*, 151–154. (b) Buchler, J. W.; Rohbock, K. *Inorg. Nucl. Chem. Lett.* **1972**, *8*, 1073–1076. (c) Buchler, J. W.; Puppe, L.; Rohbock, K.; Schneehage, H. *Chem. Ber.* **1973**, *106*, 2710–2732. (d) Johnson, J. F.; Scheidt, W. R. *J. Am. Chem. Soc.* **1977**, *99*, 294–295; *Inorg. Chem.* **1978**, *17*, 1280–1287.

(14) For a review see: Murray, K. S. *Coord. Chem. Rev.* **1974**, *12*, 1–35.

(15) Vogt, L. H., Jr.; Zalkin, A.; Templeton, D. H. *Inorg. Chem.* **1967**, *6*, 1725–1730.

(16) (a) Scheidt, W. R.; Summerville, D. A.; Cohen, I. A. *J. Am. Chem. Soc.* **1976**, *98*, 6623–6628. (b) Summerville, D. A.; Cohen, I. A. *Ibid.* **1976**, *98*, 1747–1752. (c) For other $\mu$-nitrido structures see: $Ru_2NCl_8(H_2O)_2^{3-}$, Ciechanowicz, M.; Skapski, A. C. *J. Chem. Soc. A* **1971**, 1792–1794. Gee, R. J. D.; Powell, H. M. *Ibid.* **1971**, 1795–1797. $W_2NCl_{10}^{2-}$, Weller, F.; Liebelt, W.; Dehnicke, K. *Angew. Chem.* **1980**, *92*, 211–211. $Os_2N[S_2CN(CH_3)_2]_5$, Given, K. W.; Pignolet, L. H. *Inorg. Chem.* **1977**, *16*, 2982–2984. $Ta_2NBr_{10}^{2-}$, Frank, K.-P.; Strähle, J.; Weidlein, J. *Z. Naturforsch., B: Anorg. Chem., Org. Chem.* **1980**, *35B*, 300–306. (d) Carbonyl clusters containing interstitial nitrogen, $[M_6N(CO)_{15}]^-$ (M = Co, Rh), have been reported: Martinengo, S.; Ciani, G.; Sironi, A.; Heaton, B. T.; Mason, J. *J. Am. Chem. Soc.* **1979**, *101*, 7095–7097.

(17) Gerlock, M.; McKenzie, E. D.; Towl, A. D. C. *J. Chem. Soc. A* **1969**, 2850–2858.

(18) (a) Dunitz, J. D.; Orgel, L. E. *J. Chem. Soc.* **1953**, 2594–2596. (b) Jezowska-Trzebiatowska, B. *Pure Appl. Chem.* **1971**, *27*, 89–111 and references therein. (c) Hay, P. J.; Thibeault, J. C.; Hoffmann, R. *J. Am. Chem. Soc.* **1975**, *97*, 4884–4899. Hoffmann, R.; Chen, M. M. L.; Elian, M.; Rossi, A. R.; Mingos, D. M. P. *Inorg. Chem.* **1974**, *13*, 2666–2675. (d) Burdett, J. K. *Ibid.* **1978**, *17*, 2537–2552.

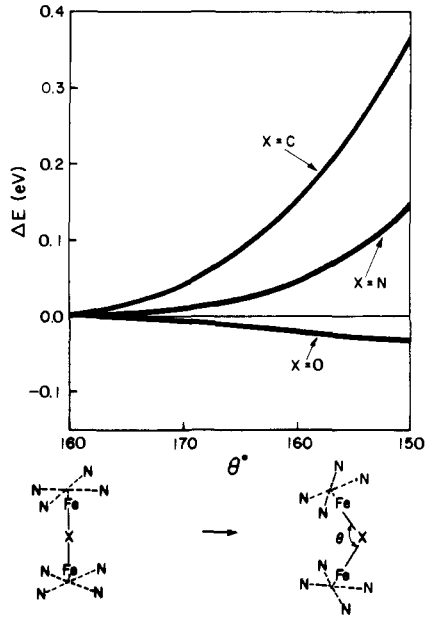


**Figure 4.** Potential energy curves calculated for Fe–X–Fe bending of the single-atom-bridged dimers $N_4Fe$–X–$FeN_4$, X = C, N, and O.

recent ESCA study on the nitrido-bridged dimer[19] shows a sharp Fe 2p photoelectron peak, indicating low-spin character of the iron on the complex. From our calculations, we cannot predict with assurance which of the four nearly degenerate orbitals $a_1$, $b_2$, and $e_1$ accepts the odd electron. But we can say something about the distribution of electron density in each candidate. Among these orbitals, the $a_1$ is primarily metal centered, 44.5% on each Fe, the mixing with nitrido 2s being only 1.6%. The $e_1$ has the largest nitrido 2p admixture of 25.7%, with 33.9% on each Fe while the $b_2$ is 11.3% on nitrido 2p and 40.1% on each Fe. We hope that this information will aid in assigning the symmetry of the half-occupied level of $(Fe–TPP)_2N$, in some future study by, for instance, EPR.

Figure 3 shows how the valence orbitals of $(Fe–N_4)_2X$ vary when the bridging atom N is replaced by O or C. For $(Fe–N_4)_2O$, the out-of-plane displacement of Fe (0.5 Å) and the Fe–O distance (1.763 Å) are taken from the X-ray diffraction data of $(Fe–TPP)_2O$,[11a] corresponding geometrical parameters for $(Fe–N_4)_2C$ being assumed similar to those for $(Fe–TPP)_2N$. The high-lying unoccupied $e_2$ level is omitted in Figure 3. As the bridging group is varied, the position of the $a_1$ and the low-lying $e_2$ and $e_3$ remains relatively constant, but the energy of the $b_2$ and $e_1$ orbitals varies significantly. As one proceeds from O to N to C, the 2p orbitals are both closer in energy to and have a better overlap with the metal 3d, destabilizing the metal d block orbitals, especially $e_1$, more. For X = O, the $e_1$ becomes the lowest among the higher four d orbitals, where the four levels are still close to each other, lying within 0.5 eV of each other. This must be why the magnetic behavior of the iron–$\mu$-oxo complexes is somewhat complicated,[16,20] for their four closely related levels are available for the two last electrons.

The most striking aspect of the level scheme of Figure 3 is that it suggests the existence of a low-spin complex with one electron less than $\mu$-N and two electrons less than $\mu$-O. Such a situation of eight electrons from $\mu$-X and eight d-block electrons from the two metals can be achieved in three distinct ways. One can doubly oxidize an $Fe^{III}(Fe–TPP)_2O$,[21] though the problem of the actual spin ground state of that system is not resolved. Or one can move to another metal or ligand set, as in (Mn–phthalocyanine)$_2$O·(py)$_2$[15] (**8b**) or $(RuCl_5)_2O·H_2O^{4-}$[22] (**10**). But most interesting

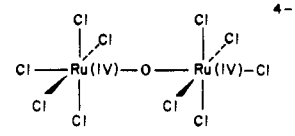


**10**

is retention of the iron group metal atom but formal oxidation of the bridge, i.e., $(Fe–TPP)_2C$ (**11a**) or some equivalent $L_nFe^{IV}–C–Fe^{IV}L_n$ (**11b,c**).

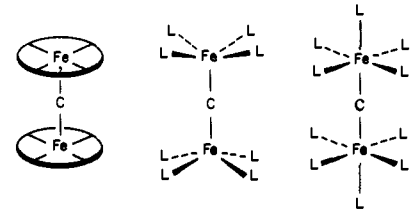


**11a** **11b** **11c**

Carbides in which a carbon atom is encapsulated by a metal polyhedron are now well-known.[23] Simple carbon sandwiches have been occasionally proposed,[24a,b] but we know of no authentic example.[24c] Our suggestion of a stable, diamagnetic, carbon sandwich $(Fe–TPP)_2C$ might be considered outlandish, were it not for the fact that precisely this molecule has just been made. Mansuy and co-workers,[25] quite independently of our theoretical work, have synthesized $(Fe–TPP)_2C$ by several routes as shown in eq 1–4. The molecule is diamagnetic and quite stable.

$$2Fe(TPP) + CI_4 \xrightarrow{+ne^-} (Fe–TPP)_2C \quad (1)$$

$$2Fe(TPP) + (CH_3)_3SiCCl_3 \xrightarrow{+ne^-} (Fe–TPP)_2C \quad (2)$$

$$2Fe(TPP) + CH_2Cl_2 + n\text{-BuLi} \rightarrow (Fe–TPP)_2C \quad (3)$$

$$Fe(TPP) + Fe(TPP)(CBr_2) \xrightarrow{+2e^-} (Fe–TPP)_2C \quad (4)$$

The number of electrons in the M–X antibonding orbitals $a_1$, $b_2$, or $e_1$ decreases in the order of X = O > N > C which, in turn, leads to an increasing order O < N < C of M–X net bonding interactions. If the ground electronic configurations are $(e_2^4e_3^4e_1^2a_1^0b_2^0)$ for X = O, $(e_2^4e_3^4a_1^1e_1^0b_2^0)$ for X = N, and $(e_2^4e_3^4a_1^0b_2^0e_1^0)$ for X = C, calculated Fe–X overlap populations are 0.44, 0.88, and 1.08, respectively. In the carbido-bridged dimer the $\pi$ overlap population between Fe ($xz + yz$) and C ($x + y$) orbitals amounts to 0.41, indicating the presence of strong Fe–C $\pi$ bonding.

One may recall here also the recently synthesized $\mu$-chloro-iron(III)-(porphyrin)copper(II) complex [(Fe–porphyrin)–Cl–$Cu(N)_4]^{2+}$[26] (**12**). The Fe(III)–Cl–Cu(II) spine has four more

(19) Kadish, K. M.; Bottomley, L. A.; Brace, J. G.; Winograd, N. *J. Am. Chem. Soc.* **1980**, *102*, 4341–4344. See, however, Schick, G. A.; Boclan, D. F. *Ibid.* **1980**, *102*, 7982–7983.

(20) (a) Lewis, J.; Mabbs, F. E.; Richards, A. *Nature (London)* **1965**, *207*, 855–856; *J. Chem. Soc. A* **1967**, 1014–1018. (b) Reiff, W. M.; Long, G. L.; Baker, W. A., Jr. *J. Am. Chem. Soc.* **1968**, *90*, 6347–6351. (c) Fleischer, E. B.; Palmer, J. M.; Srivastava, T. S.; Chatterjee, A. *Ibid.* **1971**, *93*, 3162–3167. (d) Schugar, H. J.; Rossman, G. R.; Barraclough, C. G.; Gray, H. B. *Ibid.* **1972**, *94*, 2683–2690. (e) Wollmann, R. G.; Hendrickson, D. N. *Inorg. Chem.* **1977**, *16*, 723–733. (f) For magnetic properties of sulphido-bridged iron(III) Schiff bases see: Mitchell, P. C. H.; Parker, D. A. *J. Inorg. Nucl. Chem.* **1973**, *35*, 1385–1390.

(21) Phillippi, M. A.; Goff, H. M. *J. Am. Chem. Soc.* **1979**, *101*, 7641–7643.

(22) Matheson, A. M.; Mellor, D. P.; Stephenson, N. C. *Acta Crystallogr.* **1952**, *5*, 185–186.

(23) (a) Mason, R.; Robinson, W. R. *J. Chem. Soc., Chem. Commun.* **1968**, 468–469. (b) Braye, E. H.; Dahl, L. F.; Hübel, W.; Wampler, D. L. *J. Am. Chem. Soc.* **1962**, *84*, 4633–4639. (c) The most recently published paper is the following: Tachikawa, M.; Sievert, A. C.; Muetterties, E. L.; Thompson, M. R.; Day, C. S.; Day, V. W. *Ibid.* **1980**, *102*, 1725–1727 and references therein.

(24) (a) Collins, J. B.; Schleyer, P. v. R. *Inorg. Chem.* **1977**, *16*, 152–155. Jemmis, E. D.; Schleyer, P. v. R., private communication. (b) Minkin, V. I.; Minyaev, R. M. *Zh. Org. Khim.* **1979**, *15*, 225–234. (c) There is an intriguing report, accompanied by a crystal structure, of $Sn(TPP)(Re(CO)_3C)_2$ in which carbides are sandwiched between Re and Sn: Noda, I.; Kato, S.; Mizuta, M.; Yasuoka, N.; Kasai, N. *Angew. Chem.* **1979**, *91*, 85–86. Our calculations on this structure do not lead to a satisfactory electronic configuration, and we are led to wonder if the carbide atom might be really O or $CH_2$.

(25) Mansuy, D. *Pure Appl. Chem.* **1980**, *52*, 681–690. Mansuy, D.; Lecomte, J. P.; Chottard, J. C.; Bartoli, J. F., to be submitted for publication.

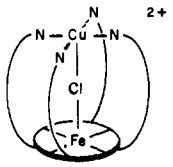

12

electrons than $(Fe–TPP)_2O$. The additional electrons should sit in M–Cl antibonding orbitals which would be similar to the $e_1$, $b_2$, and $a_1$ orbitals in $(Fe–TPP)_2X$. This will result in a substantial weakening of M–Cl bonds and explain the long Fe–Cl (2.55 Å) and Cu–Cl (2.41 Å) bond distances observed by X-ray diffraction analysis. The instability of a chlorine atom in the bridging position may be seen in the infrared spectrum, which shows a strengthening of the Fe–Cl bond at a lower temperature, indicating a shift of the Cl atom toward Fe.

We have studied the bending of $(Fe–N_4)_2X$ (X = O, N, C), i.e., variation of the Fe–X–Fe angle $\theta$. Potential energy curves are shown in Figure 4, where low-spin configurations are assumed for both X = O and N. The $\mu$-oxo compound has a very soft surface with a tendency to bend. The Fe–O–Fe = 150° geometry, the most bent geometry we calculated, is preferred to the "linear" spine by less than 1 kcal/mol. A potential minimum will be found at an angle $\theta$ somewhere smaller than 150°. In the actual porphyrin dimers $(Fe–TPP)_2O$, the observed Fe–O–Fe angle is 174.5°. This reflects a limit to the amount of steric interaction that can occur between the two TPP rings. Our $N_4$ model porphyrin obviously lacks the steric bulk that real porphyrins have. With respect to the bending, our model might represent better $\mu$-oxo-iron(III) Schiff-base dimers. The electronic structure of these is equivalent to $(Fe–TPP)_2O$, but they possess greater geometrical flexibility in their macrocycles. When the steric demands of the ligand sphere allow it, e.g., $(Fe–salen)_2O$, the Fe–O–Fe spine can bend up to 139°.[27] Other isoelectronic systems, which exhibit notable M–O–M bending, include $enH_2[(Fe^{III}–HEDTA)_2O]\cdot 6H_2O$,[28] (165°) and $[(bpy)_2(NO_2)Ru^{III}]_2O\cdot(ClO_4)_2\cdot 2H_2O$[29] (157.2°).

Let us trace the factors responsible for these bending curves through a Walsh diagram, drawn schematically in **13**. In the

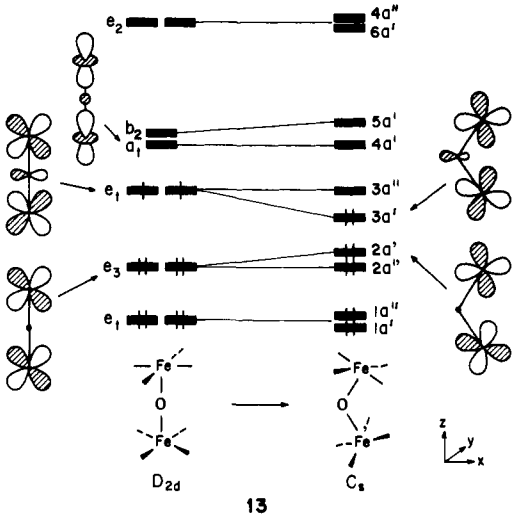


13

lowest and the highest portion of the diagram two $\delta$-type orbital sets, $e_2$, remain at their initial energy. The position of the $a_1$ level is almost unchanged, while the $b_2$ is slightly destabilized. The important orbital energy changes occur in $e_1$ and $e_3$. In these, the components in the $xz$ plane, which turn to a′ in the lowered $C_s$ symmetry, are affected by the bending motion. The 3a′ from $e_1$ favors bending, possibly due to (1) an increasing bonding interaction between Fe $xz$ orbitals and/or (2) a hybridization of O 2s with 2p which may enfeeble the Fe–O antibonding character. The O 2s–2p hybridization may be expressed in terms of an $e_1$–$a_1$ MO mixing in the lower symmetry. The 2a′ from $e_3$, on the other hand, resists bending because of an increasing Fe–Fe antibonding interaction. Another factor opposing bending comes from "core" levels below the d block, where ligand–ligand steric repulsions are to be seen. The net balance of these opposing effects is that the stabilization of $e_1$ overcomes, ever so slightly, the latter two destabilizing factors.

The analysis of the Walsh diagram points out that the nonlinear geometry of the $d^5$–$d^5$ M—O—M framework is rather unique among $\mu$-oxo dimers. If two or more electrons are removed from the Fe(III)—O—Fe(III), there will be no occupied valence orbital favoring a bent form. This should lead to a linear M—O—M framework. In fact the linear geometry has been observed for all $\mu$-oxo dimers of $d^n$–$d^n$ ($n < 5$) electron systems, e.g., $[(Cr(NH_3)_5)_2O]Cl_4\cdot H_2O$ ($d^3$–$d^3$),[30] (py—Mn—Pc)$_2$O ($d^4$–$d^4$),[15] (O=Mo—TPP)$_2$O ($d^1$–$d^1$),[13] $K_4[(RuCl_5)_2O]\cdot H_2O$ ($d^4$–$d^4$) (**10**),[22] $K_4[(ReCl_5)_2O]\cdot H_2O$ ($d^3$–$d^3$),[31a] and $Re_2O_3(dtc)_2$ ($d^2$–$d^2$).[31b]

Now return to Figure 4. The $\mu$-nitrido model complex $(Fe–N_4)_2N$ favors a linear Fe–N–Fe spine, in agreement with the observed $(Fe–TPP)_2N$ structure. The Walsh diagram for bending the $\mu$-nitrodo model (see **14**) is slightly different from that of the

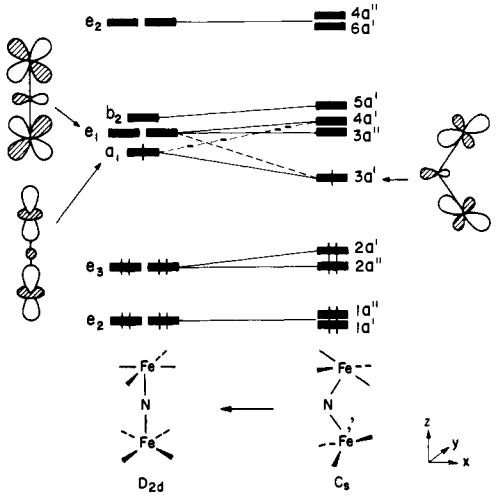


14

$\mu$-oxo complex. The highest occupied level (HOMO) is now $a_1$. The $a_1$, in which an odd electron resides, favors bending, while the $e_1$ level shows no significant change in its orbital energy. The stabilization of the $a_1$ level should arise from N 2s–2p hybridization, in other words, from the $a_1$–$e_1$ molecular orbital mixing. Other orbitals behave in the same way as corresponding orbitals in $\mu$-oxo compound do. Thus the origin of the geometrical contrast between $\mu$-oxo- and $\mu$-nitrido-iron complexes may be ascribed to the different number of electrons in the d block. Two electrons in $e_1$ of $\mu$-oxo complex (see **13**) are responsible for its preference of a bent geometry. For $\mu$-nitrido, on the other hand, only one electron in the $a_1$ level seeks a bent form but cannot compensate the opposing effects of both $e_3$ and the core levels, which prefer linearity.

It should be noted that the conclusions as to the linearity of the nitrido complex do not depend on the precise level ordering.

(26) Gunter, M. J.; Mander, L. N.; McLaughlin, G. M.; Murray, K. S.; Berry, K. J.; Clark, P. E.; Buckingham, D. A. *J. Am. Chem. Soc.* **1980**, *102*, 1470–1473.

(27) (a) See Table 3 in ref 14 and references in the footnotes. (b) (Fe-2-Mequin)$_2$O (Fe–O–Fe = 151.6°): Mabbs, F. E.; McLachlan, V. N.; McFadden, D.; McPhail, A. T. *J. Chem. Soc., Dalton Trans.* **1973**, 2016–2021.

(28) Lippard, S. J.; Schugar, H. J.; Walling, C. *Inorg. Chem.* **1967**, *6*, 1825–1831.

(29) Phelps, D. W.; Kahn, E. M.; Hodgson, D. J. *Ibid.* **1975**, *14*, 2486–2490.

(30) (a) Yewitz, M.; Stanko, J. A. *J. Am. Chem. Soc.* **1971**, *93*, 1512–1513. (b) Urushiyama, A.; Nomura, T.; Nakahara, M. *Bull. Chem. Soc. Jpn.* **1970**, *43*, 3971; *Ibid.* **1972**, *45*, 2406–2412. (c) Pedersen, E. *Acta Chem. Scand.* **1972**, *26*, 333–342.

(31) (a) Morrow, J. C. *Acta Crystallogr.* **1962**, *15*, 851–855. (b) Fletcher, S. R.; Rowbottom, J. F. Skapski, A. C.; Wilkinson, G. *J. Chem. Soc., Chem. Commun.* **1970**, 1572–1573. Fletcher, S. R.; Skapski, A. C. *J. Chem. Soc., Dalton Trans.* **1972**, 1073–1078.

We have the odd electron in $a_1$, but as we mentioned above there are four levels ($a_1$, $e_1$, $b_2$) close to each other, and it could well be that the details of porphyrin structure will so conspire as to put the odd electron into a level other than $a_1$. That is not likely to affect the Walsh diagram. Note that in that little subblock of levels one a' (3a') goes down in energy with bending, one goes up, and one stays put. This pattern is typical of orbitals interacting with some symmetry lowering distortion when they could not interact in the absence of that distortion. It is probable that such a pattern (one up, one down, one constant) will be obtained no matter what the level ordering.

When the odd electron is removed from the system, the singly oxidized $\mu$-nitrido-porphyrin dimers must have a linear structure. Although there is no direct example of this type, an analogous compound of the same electron count may be $Ru_2NCl_8(H_2O)_2^{3-}$. It does possess, indeed, a linear Ru–N–Ru bond (see **15**).[16c]

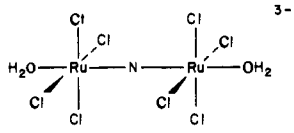


**15**

In Figure 4, the $\mu$-carbido complex exhibits clearly its preference for a linear Fe–C–Fe geometry. The explanation for the potential curve is straightforward, from Figure 3 and from the Walsh diagrams **13** and **14**. There is no electron in the higher d block for X = C. No matter how these unoccupied d levels behave, all occupied orbital sets oppose the bending motion. We predict that the Fe–C–Fe bond in a $\mu$-carbido-iron–porphyrin dimer should be linear.

**Dioxygen-Bridged Porphyrin Dimers.** Since the early discovery[32] of the synthetic dioxygen cobalt complex $[(NH_3)_5Co–O–O–Co(NH_3)_5]^{4+}$, a vast number of dioxygen-bridged cobalt dimers have been reported.[33,34] The parent cobalt compounds are mostly classical inorganic types, e.g., Werner-type $[Co(CN)_5]^{3-}$ or Schiff-base type Co(salen)(py), while cobalt-porphyrin dimers are relatively rare.[35] In naturally occurring systems, hemerythrins and hemocyanines are believed to have a M–O–O–M skeleton, where M = Fe for the former and M = Cu for the latter. Neither of them, however, contains a porphyrin moiety.

Dioxygen-bridged iron–porphyrin dimers have often been proposed as an intermediate in the autoxidation of ferrous porphyrins leading to the final oxidation product, the previously discussed $\mu$-oxo dimer (Fe–porphyrin)$_2$O.[36] The formation of an Fe–O–O–Fe intermediate was recently confirmed by La Mar, Balch, and co-workers.[37] Introduction of dry $O_2$ into toluene solutions of Fe–(*m*-tolyl–TPP) results in the formation of the $\mu$-dioxo dimer (Fe–*m*-tolyl–TPP)$_2O_2$ which is characterized by $^1$H NMR and magnetic data. Interestingly these solutions are stable indefinitely at −80 °C (≥weeks) and for ~1 h at −30 °C.

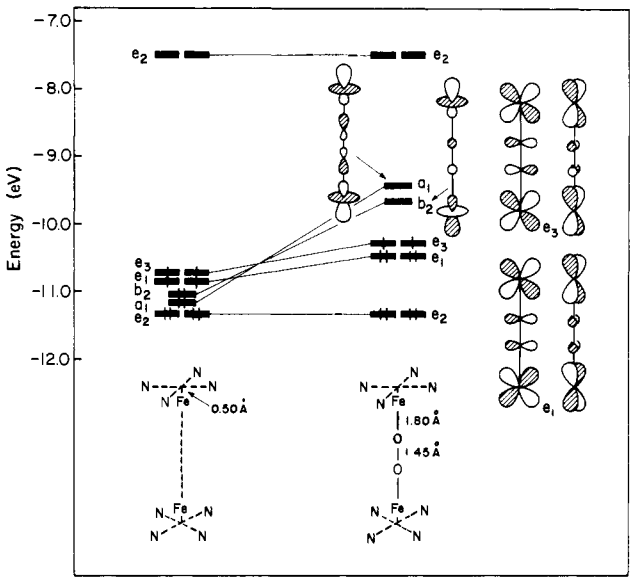


**Figure 5.** The building up of the orbitals of $N_4Fe–O–O–FeN_4$ with a linear Fe–O–O–Fe spine. At the left there are ten d orbitals of two $FeN_4$ units separated by 5.05 Å. Then the orbitals of the $(FeN_4)_2$ composite are allowed to interact with the $O_2$ orbitals at the right.

We show, in Figure 5, the orbital interaction diagram for a model iron–porphyrin dimer and dioxygen, where the Fe–O–O–Fe skeleton is linear. The two Fe–$N_4$ units are put in a staggered position, thus the $D_{4d}$ molecular symmetry. Other geometrical parameters used are Ct–Fe = 0.5 Å, Fe–O = 1.80 Å, and O–O = 1.45 Å. Two pyramidal Fe–$N_4$ units, which are separated by 5.05 Å from each other, provide a set of eight low-lying d orbitals in the first column of Figure 5. Of the orbitals of bridging $O_2$, $\pi$ ($e_1$), $\pi^*$ ($e_3$), and in- and out-of-phase combinations of lone-pair orbitals ($a_1$, $b_2$) are responsible for the interactions with the low-lying d block. Since the half or doubly occupied $O_2$ orbitals are all lower in energy than the d block, the insertion of $O_2$ in between two Fe–$N_4$ units pushes six d block orbitals up by different amounts, 0.4–1.6 eV. These destabilized d orbitals are antibonding combinations of $O_2$ and Fe d orbitals. Of these $a_1$ and $b_2$ are most destabilized by an interaction with $O_2$ lone pairs. The $O_2$ $\pi^*$–$d_\pi(xz, yz)$ interaction $e_3$ is slightly stronger than $O_2$ $\pi$–$d_\pi$ interaction $e_1$. The d orbitals of $\delta$ symmetry, $e_2$, remain unaffected by any of $O_2$ orbitals as in the case of single atom-bridged porphyrin dimers, $(Fe–N_4)_2X$.

Electron counting in dioxygen complexes is always complicated by the neutral dioxygen vs. peroxide dichotomy. The fragment electrons are placed in Figure 5 as if the fragments were $O_2$ neutral and two $d^6$ $ML_4$ fragments, $Fe(NH_2)_4^{2-}$. Electron transfer to the $O_2$ $\pi^*$ is extensive, and one could just as well think of this system as peroxide and two $d^5$ centers, thus accounting for the ten electrons in the d block of the composite molecule. The electron count here is thus appropriate to a model for $(TPP–Fe)_2O_2$.

The actual complexes are not likely to be linear, and one might delay a discussion of their magnetic properties until the question of nonlinearity is treated in detail. However, it will turn out that bending at oxygen does not have a major effect on the orbital energies, so that most fundamentals of the level scheme can be discussed on the basis of Figure 5. Specifically note the rather small HOMO–LUMO gap of ~0.6 eV. This may leave one with the uncertainty as to whether the $d^5$–$d^5$ dimers under discussion might show a further unpairing of electrons, beyond the triplet

(32) Werner, A.; Mylius, A. *Z. Anorg. Chem.* **1898**, *16*, 245–267.

(33) Detailed discussions of dioxygen-bridged cobalt dimers are given in recent review papers on synthetic oxygen carriers: (a) McLendon, G.; Martell, A. E. *Coord. Chem. Rev.* **1976**, *19*, 1–39. (b) See a review by R. D. Jones et al. in ref 2a.

(34) Some recently published papers on $\mu$-oxo-cobalt dimers include the following: Timmons, J. H.; Niswander, R. H.; Clearfield, A.; Martell, A. E. *Inorg. Chem.* **1979**, *18*, 2977–2982. Pickens, S. R.; Martell, A. E.; *Ibid.* **1980**, *19*, 15–21. Harris, W. R.; McLendon, G. L.; Martell, A. E.; Bess, R. C.; Mason, M. *Ibid.* **1980**, *19*, 21–26.

(35) (a) See ref 2h and references therein. (b) Chang, C. K. *J. Chem. Soc., Chem. Commun.* **1977**, 800–801.

(36) For example: (a) Sadasivan, N.; Eberspaecher, H. I.; Fuchsman, W. H.; Caughey, W. S. *Biochemistry* **1969**, *8*, 534–541. Alben, J. O.; Fuchsman, W. H.; Beaudreau, C. A.; Caughey, W. S. *Ibid.* **1968**, *7*, 624–635. Cohen, I. A.; Caughey, W. S. "Hemes and Hemoproteins"; Chance, B.; Easterbrook, R. E.; Yonetani, T., Ed.; Academic Press: New York, 1966, pp 577–579. Cohen, I. A.; Caughey, W. S. *Biochemistry* **1968**, *7*, 636–641. (b) Ochiai, E.-I. *Inorg. Nucl. Chem. Lett.* **1974**, *10*, 453–457. (c) A dioxygen unit bridging between $Fe^{III}$(porphyrin)(Imid) and Cu(II) is a model postulated for cytochrome oxidases: Petty, R. H.; Welch, B. R.; Wilson, L. J.; Bottomley, L. A.; Kadish, K. M. *J. Am. Chem. Soc.* **1980**, *102*, 611–620 and see references therein. (d) Also bimetallic dioxygen adducts containing both cobalt and molybdenum were synthesized during a study of model compounds for olefin autoxidation catalysts: Arzoumanian, H.; Alvarez, L. R.; Kovalak, A. D.; Metzger, J. *J. Am. Chem. Soc.* **1977**, *99*, 5175–5176. Arizoumanian, H.; Lai, R.; Alvarez, R. L.; Petrignani, J.-F.; Metzger, J.; Fuhrop, J. *Ibid.* **1980**, *102*, 845–847.

(37) Chin, D.-H.; Gaudio, J. D.; La Mar, G. N.; Balch, A. L. *J. Am. Chem. Soc.* **1977**, *99*, 5486–5488. Chin, D.-H.; Balch, A. L.; La Mar, G. N. *Ibid.* **1980**, *102*, 1446–1448.

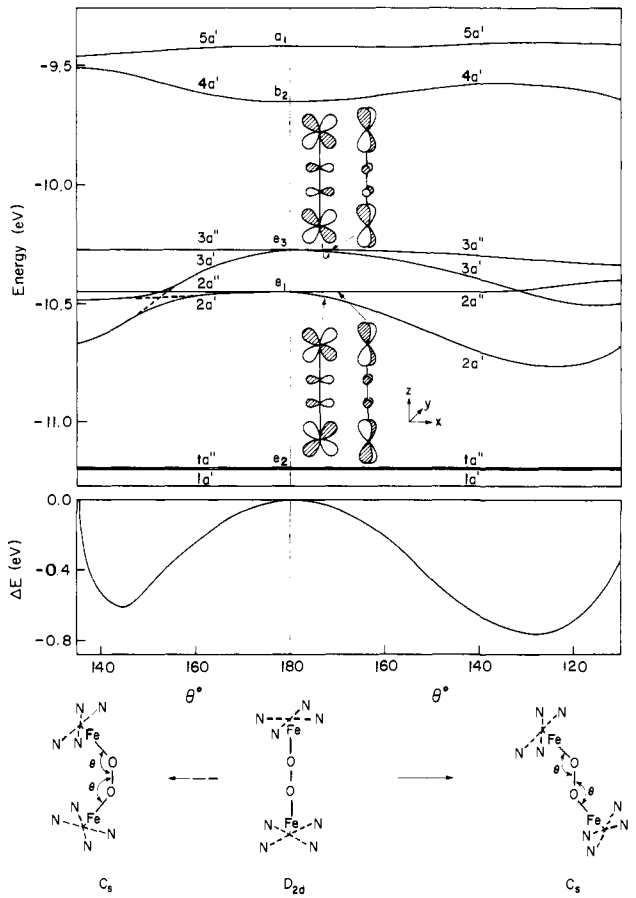


**Figure 6.** Walsh diagram (top) and the total energy curve (bottom) for cis and trans bending of $N_4Fe$–O–O–$FeN_4$. The electronic configuration assumed for calculation of total energies is a closed shell singlet.

state implied by the orbital filling of Figure 5. However, when the metal atoms take up bases (i.e., $\sigma$ donors) at the axial position (see **16**), the $a_1$ and $b_2$ levels will be pushed up significantly, leading

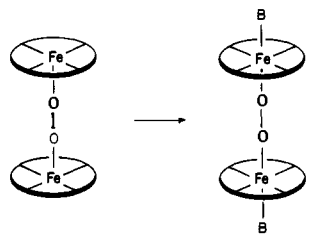


**16**

to a certain intermediate (triplet) spin state. The magnetism of dioxygen-bridged dimers will be discussed below.

It is known that the stable geometry of $O_2$-bridged cobalt dimers does not have a linear Co–O–O–Co skeleton, but instead this unit takes on a zig-zag form. If we regard the bridging dioxygen as peroxide $O_2^{2-}$, the cobalt–$\mu$-peroxo complexes are all Co(III) $d^6$–Co(III) $d^6$ dimers. The structures of the interesting $d^5$–$d^5$ Fe(III)–Fe(III) porphyrin dimers are as yet unknown. It is thus interesting to explore theoretically the structures of these molecules. We have performed calculations for $(Fe–N_4)_2O_2$, varying the two Fe–O–O angles $\theta$ simultaneously. There are two ways for doing this: one is trans bending and the other is cis bending. Figure 6 plots the change in the total energy vs. the angle $\theta$, assuming a low-spin state for $(Fe–N_4)_2O_2$. For the model porphyrin compound, both cis and trans bent geometries are favored to a different extent compared to the linear form. The energy minimum for the trans bending is calculated to come at about 127°. The potential curve for cis bending is very similar to that for trans bending until the compound meets a serious steric problem at around 146°. Although real porphyrins are much bulkier than the model, we expect that the cis bent structure is also a realistic structural possibility, if the steric constraints allow it.

The variation in energy of the eight d-block orbitals as a function of $\theta$ is also drawn in Figure 6. Because the molecular symmetry is reduced from $D_{4d}$ to $C_s$, the cis and trans deformations split each of three degenerate orbitals $e_2$, $e_1$, and $e_3$ into a′ and a″ levels. The lowest $e_2$ level, which is a d orbital combination of $\delta$ symmetry, does not change its energy as $\theta$ is varied. Also 2a″ (from $e_1$) and 3a″ (from $e_3$) are indifferent to the bending and retain their $\pi$-orbital character with respect to the $xy$ plane. Thus the driving force for the deformation may be traced entirely to the stabilization of two a′ orbitals which arise from $e_1$ and $e_3$.

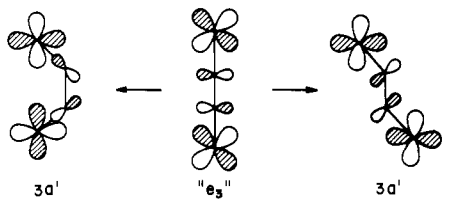


**17**

First let's consider the variation of $e_3 \rightarrow 3a'$ orbital **17** which, in the linear form, consists of an antibonding combination of Fe $d_{xz}$ with O $p_x$. For the trans deformation, the oxygen $p_x$ orbitals follow the bending motion of the adjacent $d_{xz}$ orbitals keeping $d_\pi$–O $p_x$ antibonding interactions. Another way of saying this is that both O $p_x$ orbitals rotate anticlockwise by about the same amount as the Fe–$N_4$ units twist. This type of reorientation of O $p_x$ orbitals does not relieve the $d_{xz}$–O $p_x$ antibonding character but reduces $O_2$ $\pi^*$ antibonding interaction or increases $O_2$ $\sigma$-bonding interaction. This is the way the 3a′ is stabilized by trans bending. Cis bending on the other hand, induces O $p_x$ rotations in a different direction: one in a clockwise and the other in an anticlockwise manner. The Fe $d_\pi$–$O_\pi$ repulsive interaction is then removed, while $O_2$ $\sigma^*$ character is added. These are opposing effects on the 3a′ energy level. The balance results in a large stabilization of 3a′. In a similar way the origin of 2a′ stabilization can be seen in **18**.

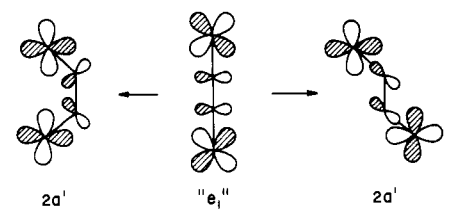


**18**

Fe $d_\pi$–O $p_\pi$ antibonding interactions in 2a′ are decreased for trans and an $O_2$ $\sigma$ contribution is increased for cis. The analysis of these orbital trends is not simple. It can be put on a firmer footing with the aid of second-order perturbation-theoretic arguments—it is ultimately a mixing of oxygen lone pairs and $\pi$ orbitals which is responsible for the reorientation of the $\pi^*$'s in the lower symmetry—but we do not think it is worth presenting here.

As a consequence of the $e_3$ and $e_1$ level splitting, 3a″ becomes the LUMO of $(Fe–N_4)_2O_2$ in a bent form, and the HOMO is 3a′ at small $\theta$ or 2a″ at large $\theta$. Important features in Figure 6 are a very small HOMO–LUMO energy gap and a flat curve of the LUMO over the whole range of $\theta$. The small HOMO–LUMO separation is probably behind the temperature dependence of the magnetic moment[37] and also accounts in a qualitative way for the kinetic instability of the Fe(III)–O–O–Fe(III) skeleton. Conversely, M–O–O–M systems with two more electrons than $(Fe^{III}–N_4)_2O_2$ should be stable compounds, possibly diamagnetic. Addition of axial ligands on the metals (**15**) would assure diamagnetism, due to an increase in $e_3$–($b_2$, $a_1$) or 3a″–(4a′, 5a′) energy separation. This is the property which we see in $\mu$-peroxo cobalt(III) dimers. One-electron oxidation of the $\mu$-peroxo cobalt(III) complexes readily yields $\mu$-superoxo complexes, Co(III)–$O_2^-$–Co(III). The observed magnetic moment, $\mu$ = 1.6–2.02

$\mu_B$, is again in the range of a low-spin state.[38]

A compound that we find enigmatic in its magnetic properties is a disulfur-bridged ruthenium dimer $[(NH_3)_5RuSSRu(NH_3)_5]X_4 \cdot 2H_2O$, X = Cl or Br (**19**).[39] The compound is iso-

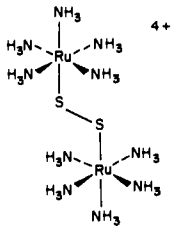

**19**

electronic with (Fe–porphyrin)$_2O_2$. Thus the Ru–S–S–Ru spine, as expected, has a trans bent form, $\theta$ = 111.5°. Reasoning from Figure 6 one might have expected a triplet ground state. A calculation on the molecule in a geometry close to experimental gives a similar pattern to the $O_2$ case but with a slightly larger HOMO–LUMO gap of 0.53 eV. We hesitate to conclude from this gap whether the molecule should be high or low spin. The dimer, X = Br, exhibits a very low and temperature-independent magnetic moment, $\mu$ = 0.45 $\mu_B$, over the range +25 to −100 °C. The magnetic moment for the related dimer *trans*-$[Cl(NH_3)_4RuSSRu(NH_3)_4Cl]Cl_2$ is 1.1 $\mu_B$ per dimer, whereas it is EPR silent in a frozen water matrix at liquid-nitrogen temperatures. We have no immediate explanation for this unusual magnetic behavior.

The flat 3a″ (LUMO) curve implies that the stable conformations of Fe(III)–O–O–Fe(III) and of M–O–O–M with one or two more electrons should be very much alike. Thus our predictions in this section for the geometry of [Fe–porphyrin]$_2O_2$ may be checked by comparison with geometries of analogous Co compounds. The observed Co–O–O angle of both $\mu$-peroxo and $\mu$-superoxo compounds ranges from 110 to 123° which is close to the number 127° calculated for our model $(Fe–N_4)_2O_2$.

Changing metals from Fe to Co is not the only way to add two electrons to the Fe–O–O–Fe skeleton. Instead, one could change the formal oxidation state of the bridging ligand. We have found only one example for this, that of the $\mu$-hydrazido-bis(heme carbonyl) derivatives.[40] The complexes are highly stable in $CDCl_3$ solution and seems to be diamagnetic. The NMR and infrared spectra indicate nonlinear OC–Fe–N–N–Fe–CO bonding (see **20**).

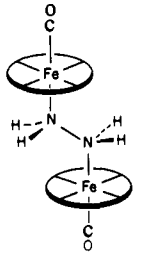

**20**

We have mentioned the possibility that a cis bent structure of (Fe–porphyrin)$_2O_2$ may exist together with the normal trans bent structure, if steric constrains allow it. Are there any cis bent dioxygen-bridged cobalt dimers? So far no structural study is available showing a cis bent Co–O–O–Co bond, except cases in which an additional $\mu$ ligand is inserted in between two Co atoms (see **21**).[41] However, we have recently been informed by

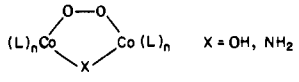

**21**

Chang[35b,42] that EPR studies on "cofacial" cobalt diporphyrins, (Co–porphyrin)$_2O_2^+$, indicate the coexistence of cis and trans isomers in the same solution (**22**).

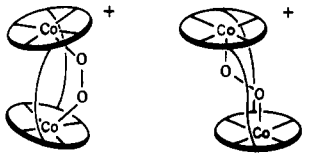

**22**

Now consider a twisting motion of two Fe–$N_4$ units around the O–O axis. In our calculations the twisting starts at a trans Fe–O–O–Fe conformation with a fixed Fe–O–O angle, $\theta$ = 120°. Then the dihedral angle $\alpha$ of the two Fe–O bonds is varied from 180 to 90°. Remarkably no particular orbital responds to the twisting motion. All valence levels keep their energies nearly constant in the range 180° ≥ $\alpha$ ≥ 90°. As a consequence the total energy curves for any electronic configuration, whatever the electron count, are very flat until a steric interaction between two Fe–$N_4$ units begins to affect the potential curve at around $\alpha$ = 110°. Therefore we think that the O–O twisting angle in any given molecule would be determined rather by steric interactions and/or crystal packing forces than by electronic factors. Experimentally the dihedral angle $\alpha$ of dimeric peroxo- and superoxocobalt complexes $(CoL_m)_2O_2^{n+}$ lies in the range of 110–180°.[33b,43] We do not find any electronic factor which rationalizes the variety of the dihedral angles observed. Interestingly, a $\mu$-superoxo complex $K_5[Co(CN)_5]_2O_2$ has both planar ($\alpha$ = 180°) and slightly nonplanar ($\alpha$ = 166°) geometries in the same crystal, indicating that packing forces play an important role in determining the angle $\alpha$.[44]

The $\mu$-peroxo and $\mu$-superoxo transition-metal dimers are not unique in showing a very flat potential surface for the twisting motion along the O–O bond. The simplest $\mu$-peroxide, i.e., hydrogen peroxide, also has a small energy barrier for going from a skewed form through trans to another skewed form, **23**, where

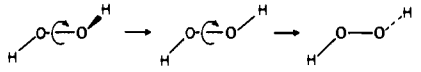

**23**

the observed equilibrium dihedral angle is 111° or 249°.[45] Experimentally the *trans* energy barrier is 1.1 kcal/mol, while calculated barriers range between 0.14 and 0.63 kcal/mol.[46]

In principle another possible geometry of $O_2$-bridged porphyrin dimers is one in which the $O_2$ is $\eta^2$ $\pi$ bonded to both metals with the O–O bond axis lying perpendicular to the metal–metal axis (see **24**). This type of structure was first proposed theoretically[47a]

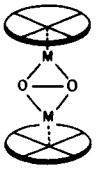

**24**

(38) See, for example: ref 33 and Duffy, D. L.; House, D. A.; Weil, J. A. *J. Inorg. Nucl. Chem.* **1969**, *31*, 2053–2058.

(39) (a) Brulet, C. R.; Isied, S. S.; Taube, H. *J. Am. Chem. Soc.* **1973**, *95*, 4758–4759. (b) Elder, R. C.; Trkula, M. *Inorg. Chem.* **1977**, *16*, 1048–1051.

(40) Caughey, W. S.; Barlow, C. H.; O'Keeffe, D. H.; O'Toole, M. C. *Ann. N.Y. Acad. Sci.* **1973**, *206*, 296–309.

(41) For examples of crystallographic structural data, see: Thewalt, U.; Marsh, R. E. *J. Am. Chem. Soc.* **1967**, *89*, 6364–6365, *Inorg. Chem.* **1972**, *11*, 351–356. Christoph, G. G.; Marsh, R. E.; Schaefer, W. P. *Ibid.* **1969**, *8*, 291–297.

(42) Chang, C. K., to be submitted for publication.

(43) The smallest dihedral angle, $\alpha$ = 110°, was observed for [Co(salen)(DMF)]$_2O_2$, Calligaris, M.; Nardin, G.; Randaccio, L.; Ripamonti, A. *J. Chem. Soc. A* **1970**, 1069–1074.

(44) Wang, B. C.; Schaefer, W. P. *Science (Washington, D.C.)* **1969**, *166*, 1404–1406.

(45) Hunt, R. H.; Leacock, R. A.; Peters, C. W.; Hecht, K. T. *J. Chem. Phys.* **1965**, *42*, 1931–1946. Hunt, R. H.; Leacock, R. R. *Ibid.* **1966**, *45*, 3141–3147.

(46) (a) Davidson, R. B.; Allen, L. C. *J. Chem. Phys.* **1971**, *55*, 519–527 and see references therein. (b) Dunning, T. H., Jr.; Winter, N. W. *Chem. Phys. Lett.* **1971**, *11*, 194–195. (c) Ranck, J. P.; Johansen, H. *Theor. Chim. Acta* **1972**, *24*, 334–345.

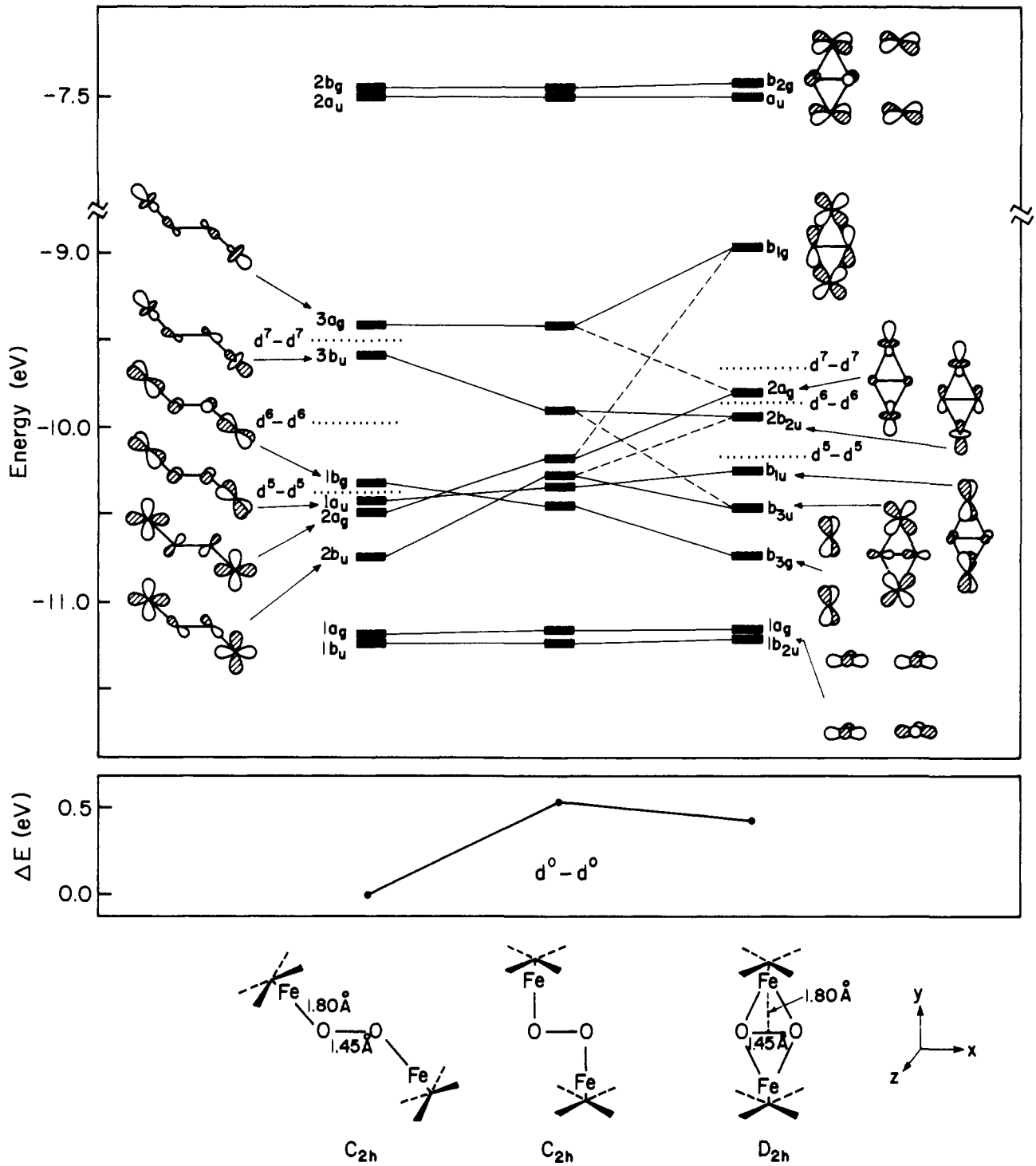


**Figure 7.** Top: Orbital correlation diagram for the deformation of $N_4Fe$–O–O–$FeN_4$ linking the two trans bent geometries, angle Fe–O–O = 120° and 90°, and the side-on structure. The $O_2$ fragment is staggered with respect to N atoms of both $N_4$ units. Dotted lines and $d^n$–$d^n$ labels indicate the filled–unfilled level gap for various d electron counts. Bottom: total energies for the $d^0$–$d^0$ electron configuration of the three geometries.

and experimentally[47b] for $[(H_3N)_5Co)]_2O_2^{5+}$. However a reinvestigation of X-ray analysis has shown that another structure is the correct one.

We have performed a calculation for the side-on structure **22** of $(Fe–N_4)_2O_2$ to see whether or not the geometry is likely for the iron–porphyrin dimers. In the calculation the distance between Fe and the center of O–O bond is assumed to be 1.80 Å, which is the same as the Fe–O distance of linear and bent $(Fe–N_4)_2O_2$. The two porphyrin rings are taken eclipsed to each other with $O_2$ being staggered with respect to the porphyrins. Other geometrical parameters are unchanged.

The right side of Figure 7 shows the valence orbital levels for this side-on structure of $(Fe–N_4)_2O_2$. Note that coordination axes have been changed, and now the $z$ axis lies perpendicular to the $Fe_2O_2$ plane. The lowest two and the highest two levels comprise levels of $\delta$ symmetry, $x^2-y^2$ and $xz$ orbitals corresponding to $e_2$ sets of linear $(Fe–N_4)_2O_2$ in Figure 5. Among others, the out-of-phase combination of $xy$, $b_{1g}$, is strongly destabilized by an antibonding interaction with $O_2$ $\pi^*$. The low-lying two vacant levels $2a_g$ and $2b_u$ consist of $y^2$. Of the three highest occupied levels $b_{1u}$ and $b_{3g}$ are derived from $yz$, and $b_{3u}$ from in-phase combination of $xy$. Some of these interactions will be familiar

(47) (a) Vlĉek, A. A. *Trans. Faraday Soc.* **1960**, *56*, 1137–1143. (b) Vannerberg, N.-G.; Brosset, C. *Acta Crystallogr.* **1963**, *16*, 247–251. (c) Marsh, R. E.; Schaefer, W. P. *Acta Crystallogr., Sect. B* **1968**, *B24*, 246–251.

to the reader acquainted with our general analysis of alternative coordination modes for diatomic molecules.[48]

At the left side of Figure 7 we plot the valence levels of trans bent $(Fe-N_4)_2O_2$, $\theta = 120°$. The levels at the middle are for $\theta = 90°$. For a higher molecular symmetry, $C_{2h}$, to be maintained for the two geometries, two porphyrins are eclipsed to each other and are staggered with respect to $O_2$. The bottom of Figure 7 gives energy sums or core levels which correspond to energies of the $d^0$–$d^0$ system. The trans bent structure with $\theta = 120°$ is close to the most stable geometry of $(Fe-N_4)_2O_2$. The minor change in conformation of the porphyrins from staggered to eclipsed does not affect the total energy and the orbital energy levels of the trans form, $\theta = 120°$. When we compare the total energy of the side-on structure of $(Fe-N_4)_2O_2$, $d^5$–$d^5$, with that of the trans bent $\theta = 120°$ form, the former is 1.1 eV higher than the latter. The relative instability of the side-on form, in our calculations, derives from two factors: (1) the $d^0$–$d^0$ energy which must reflect the increased repulsive interactions between $O_2$ and the N atoms in porphyrins and (2) destabilization of the $b_{1u}$ and $b_{3u}$ d levels.

Two-electron and four-electron reductions of the system, which are models for $d^6$–$d^6$ $(Co-N_4)_2O_2$ and $d^7$–$d^7$ $(Ni-N_4)_2O_2$ respectively, do not change the geometrical preference. The side-on form is less stable than the trans form, $\theta = 120°$, by 1.8 eV for the $d^6$–$d^6$ and by 1.4 eV for the $d^7$–$d^7$ models.

The side-on structure is competitive with an end-on bonded alternative only for low d-electron counts, $d^0$–$d^0$ to $d^3$–$d^3$. In the $d^3$–$d^3$ case there would be a level crossing between the two extreme geometries, which raises the interesting possibility of the coexistence of both isomers with a barrier to their interconversion. We will return to a molecule related to the $d^0$–$d^0$ case at the end of this section.

There are some interesting things to be learned about the relative stability or instability of side-on bonded structures from a comparison of our $(M-N_4)_2O_2$ with $H_2O_2$ and $Li_2O_2$. The "rhombic" structure of $H_2O_2$ is much less stable than the "equilateral trapezoid". Extended Hückel calculations give an energy difference of 4.4 eV.[49] The controlling factor in this preference is that the O–H bonding orbital of $a_g$ symmetry in the trapezoid $H_2O_2$ moves up strongly in energy at the rhombic form, becoming the $O_2$ $\pi^*$ level (see **25**).[50] On the other hand, the

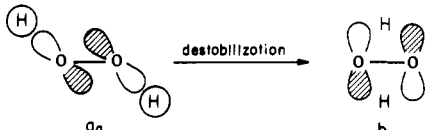


**25**

vacant Li p orbital effectively stabilizes the $b_{2g}$ in the rhombic form of $Li_2O_2$ (**26**). Thus the rhombic $Li_2O_2$ is 3.2 eV more stable than the trapezoidal one.[51]

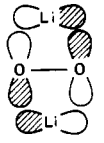

**26**

There is a similar stabilization of the $b_{2g}$ symmetry level in the side-on structure of $(Fe-N_4)_2O_2$, where the Fe $3d_{xy}$ orbitals are responsible for a bonding interaction with $O_2$ $\pi^*$. The $b_{2g}$ molecular orbital level (see **27**) is the bonding counterpart of the $b_{1g}$

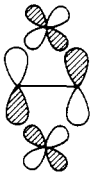

**27**

level in Figure 7, and its contribution enters the $d^0$–$d^0$ potential energy. Although the presence of such a bonding interaction between the $d_{xz}$ and $O_2$ $\pi^*$ seems to ease the instability of the side-on form, the resulting stabilization is insufficient to make this structure more stable than the trans bent geometry. Incidentally a similar stabilization has been implicated by Salem and his collaborators[52] in a proposed mechanism of coenzyme-$B_{12}$ catalyzed reactions.

One can also consider the possibility of simultaneous 1,2 migration of two model porphyrin fragments on $O_2$, as illustrated in **28**. Bond-switching organic reactions of this type have been

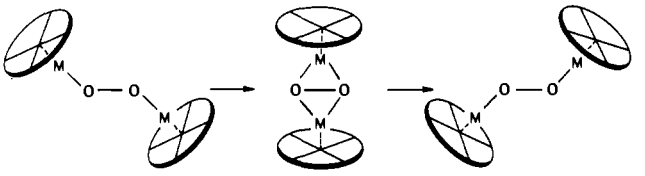

**28**

called "dyotropic" reactions.[53] Their feasibility in the ethane system has been evaluated theoretically earlier.[50] Coenzyme-$B_{12}$-catalyzed reactions may involve such a simultaneous double migration.[52] The correlation diagram required to analyze reaction **28** is already in hand in Figure 7. First there is an orbital crossing between the occupied $2a_g$ and the unoccupied $1b_g$ for the $d^5$–$d^5$ $(Fe-N_4)_2O_2$ going from the trans bent to the side-on structure. Also the $d^6$–$d^6$, which corresponds to $(Co-N_4)_2O_2$ has a level crossing between the $2a_g$ and the unoccupied $3b_u$. Second, the "reactant" $2b_u$ occupied level tends to correlate with the $2b_{2u}$ ($b_u$) of the side-on form, while the "reactant" $3b_u$ takes on the $b_{3u}$($b_u$) character. Although these levels, of course, avoid a crossing, the "reactant" $2b_u$ moves up strongly at the initial stage of the migration process. As a result the migration process of $(Fe-N_4)_2O_2$ meets an energy barrier before it reaches to the side-on structure. Thus the simultaneous 1,2 migrations of the two metal porphyrins over $O_2$ are symmetry forbidden and will require an even higher activation energy than the energy differences between the trans bent and the side-on structures. The calculated energy barriers are 1.8, 2.5, and 1.7 eV for the $d^5$–$d^5$, $d^6$–$d^6$, and $d^7$–$d^7$ configurations, respectively.

If the reader is skeptical about the advisability of any consideration of such seemingly implausible structures as a di-$\eta^2$, doubly side-on bonded dioxygen, he might take a look at the crystal structure of **29**, one product of the interaction of aluminum alkyls

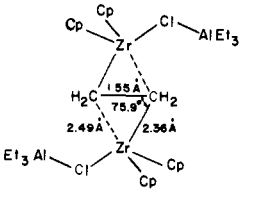


**29**

with dicyclopentadienylzirconium dihalides.[53a] The structure is

(48) Hoffmann, R.; Chen, M. M.-L.; Thorn, D. L. *Inorg. Chem.* **1977**, *16*, 503–511.

(49) Assumed geometries for the "rhombic" are O–O = 1.45 Å and H–H = 1.90 Å and for the "equilateral trapezoid" O–O = 1.45 Å, O–H = 0.95 Å, and H–O–O angle = 120°.

(50) The reader is referred to a related analysis of the instability of diborane type geometries for substituted ethanes. Hoffmann, R.; Williams, J. E., Jr. *Helv. Chim. Acta* **1972**, *55*, 67–75. An orbital symmetry analysis on dibridged ethanes and diborane structures is also available in: Gimarc, B. M. *J. Am. Chem. Soc.* **1973**, *95*, 1417–1421; *Acc. Chem. Res.* **1974**, *7*, 384–392. For an MO study of dilithioethane see: Kos, A. J.; Jemmis, E. E.; Schleyer, P. v. R.; Gleiter, R.; Fischbach, U. to be submitted for publication.

(51) Peslak, J., Jr. *J. Mol. Struct.* **1972**, *12*, 235–239. Ab initio calculations on the rhombic form are also available: Yates, J. H.; Pitzer, R. M. *J. Chem. Phys.* **1977**, *66*, 3592–3597. Kao, J. *J. Mol. Struct.* **1979**, *56*, 147–152.

(52) Salem, L.; Eisenstein, O.; Anh, N. T.; Bürgi, H.-B.; Devaquet, A.; Segal, G.; Veillard, A. *Nouv. J. Chim.* **1977**, *1*, 335–348.

(53) (a) Kaminsky, W.; Kopf, J.; Sinn, H.; Vallmer, H.-J. *Angew. Chem.* **1976**, *88*, 688–689. (b) Gell, K. I.; Williams, G. M.; Schwartz, J. *J. Chem. Soc., Chem. Commun.* **1980**, 550–552.

(54) Reetz, M. T. *J. Chem. Soc., Chem. Commun.* **1972**, *84*, 161–162; *Adv. Organomet. Chem.* **1977**, *16*, 33–65.

very close to the side-on bonded extreme. Now the $ML_n$ fragment is very different and so is the central group that is being bridged. It is ethylene, isoelectronic with $O_2$. To stay with our peroxide electron-counting convention, we might consider the central group as $CH_2CH_2^{2-}$, in which case we have a $d^0$–$d^0$ electron count. This is one of the better chances for side-on bonding for peroxide.

Just as striking as **29** is the NMR study of racemization in $(Cp_2ZrCl)_2(RHCO)$.[53b]

**Alternative Structures of (M—Porphyrin)$_2$O$_3$.** The porphyrin dimers of (M—porphyrin)$_2$O$_3$ stoichiometry show two remarkably different molecular structures. One contains a linear O=M—O—M=O group (**30**), e.g., (Mo—TPP)$_2$O$_3$.[13d] A totally different

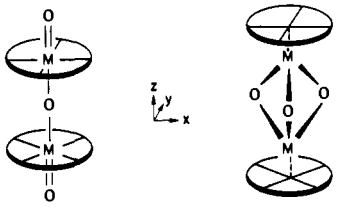

**30** **31**

geometry is found in the structure of (Nb—TPP)$_2$O$_3$[13d,55] (**31**), in which two Nb–TPP units are linked at the Nb center through three $\mu$-oxo ligands. Another geometrical contrast between these two compounds is that the Mo atom sits almost in the plane whereas the Nb moves out of the plane, toward the bridging atoms, by 1.0 Å.

An obvious difference between the electronic structure of (Mo–TPP)$_2$O$_3$ and (Nb–TPP)$_2$O$_3$ is the number of d electrons. Let us count each oxide as $O^{2-}$. Then each Mo atom in the complex has one d electron while the Nb complex has none. Is this d electron count important in determining the alternative structures? The answer is yes.

It is known that M–O $\pi$ interactions are crucial in the structure of oxo, $\mu$-oxo, $\mu$-superoxo, and $\mu$-peroxo transition-metal complexes. The most stable geometry is chosen so as to maximize the M–O $\pi$ bonding and/or to minimize the M–O $\pi^*$ antibonding interaction. For $d^0$ complexes only the former factor, the M $d_\pi$–O $p_\pi$ $\pi$ interaction, is important because M $d_\pi$–O $p_\pi$ $\pi^*$ antibonding levels are all unoccupied.

The geometry of $d^0$–$d^0$ (Nb–TPP)$_2$O$_3$ (**31**) may be rationalized in terms of maximum utilization of vacant $d_\pi$ orbitals. In the linear form **30** only two acceptor $d_\pi$ orbitals, *xz* and *yz*, of each metal atom are available for $\pi$ bonding with donor $p_x$ and $p_y$ orbitals of $O^{2-}$. The geometry **31**, on the other hand, allows vacant *xy* (or $x^2 - y^2$) and $z^2$ to partly contribute to the $\pi$ interaction, in addition to *xz* and *yz*.

Johnson and Scheidt[13d] in their structural study on (Nb–TPP)$_2$O$_3$ found that the Nb–O distances are not equal. Each Nb atom forms three distinct Nb–O bonds: one short, 1.756 Å; one long, 2.359 Å; one of intermediate length, 1.950 Å. This is drawn schematically in **32**. Interestingly the angle between the two

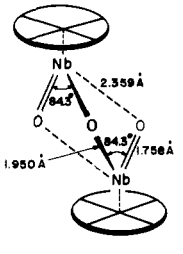


**32**

shorter Nb–O bonds of each Nb, 84.3°, is close to 90°, while the other O–Nb–O angles are smaller, ranging from 69.4 to 75.9°.

In general M $d_\pi$–O $p_\pi$ interactions are optimal when the O atoms are at 90° as shown in **33**.

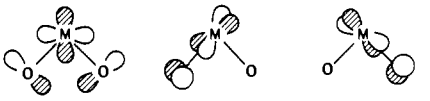

**33**

Unfortunately it is difficult to extract pure $d_\pi$–$p_\pi$ interactions from the molecular orbitals of these complexes because of the low symmetry of (Nb–TPP)$_2$O$_3$. Instead we address this problem in the $d^0$ compounds, $MoO_2$(TPP)[56] (**34**) and $MoO_3$(dien)[57] (**35**),

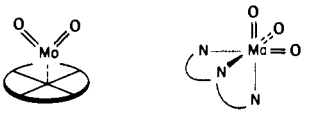

**34** **35**

which might be structurally analogous to (Nb–TPP)$_2$O$_3$ in the sense that oxygen atoms occupy cis coordination sites. The cis disposition of oxygen atoms is not a unique feature of the above two Mo compounds but in fact the prevailing trend in Mo(VI), V(V), and W(VI) $d^0$ complexes.[58] This geometrical preference has been explained in terms of maximization of M–O $\pi$ interactions.[59]

For $d^1$–$d^1$ (Mo—TPP)$_2$O$_3$ the above argument is reversed. The orbital energy of the lowest d level, the one which accepts the last two electrons, proves to be important in this case. In order to compare the energies of the lowest d level for geometries **30** and **31**, we have performed calculations on the model (Nb—N$_4$)$_2$O$_3$. For the linear O=Nb—O—Nb=O structure, each Nb atom is placed 0.1 Å out of the model porphyrin plane toward the terminal O. The Nb=O and Nb—O bond distances are 1.7 and 1.9 Å, respectively. The two $N_4$ units are staggered, thus the molecule has $D_{4d}$ symmetry. The structure of **31** consists of three planes, two model porphyrins, and $O_3$, which are parallel to and are separated by 1.3 Å from each other. The Nb atoms move out of plane by 1.0 Å. The $O_3$ forms an equilateral triangle, whose sides are 2.5 Å. The conformation is drawn in **36**. The upper

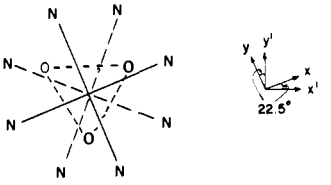


**36**

$N_4$ rotates anticlockwise by 22.5° from a staggered position with respect to $O_3$ and the lower $N_4$ rotates clockwise by the same angle. Thus two $N_4$ units are staggered.

The lowest d level is of $e_2$ symmetry for the linear (O=Nb—N$_4$)$_2$O. It is a combination of *xy* of the upper Nb—$N_4$ and $x^2 - y^2$ of the lower one. In spite of the lowered symmetry, the lowest two d orbital combinations of (Nb—N$_4$)—$O_3$—(Nb—N$_4$) retain $e_2$ character. Figure 8 plots the relative position in energy of the lowest d levels. For a comparison the $e_2$ level of a (Nb—N$_4$)$_2$ fragment is also given for each geometry.

The difference in the $e_2$ energy position between the two (Nb–N$_4$)$_2$ fragments at the right and the left ends of Figure 8 arises from a different degree of Nb out-of-plane displacement. As shown in Figure 1, a larger displacement of a central metal

(55) Lecomte, C.; Protas, J.; Guilard, R.; Fliniaux, B.; Fournari, P. *J. Chem. Soc., Dalton Trans.* **1979**, 1306–1313.

(56) Ledon, H.; Bonnet, M. *J. Chem. Soc., Chem. Commun.* **1979**, 702–704. The X-ray crystal analysis of (Mo–TPP)$O_2$ has been completed: Mentzen, B. F.; Bonnet, M. C.; Ledon, H. J. *Inorg. Chem.* **1980**, *19*, 2061–2066.

(57) Cotton, F. A.; Elder, R. C. *Inorg. Chem.* **1964**, *3*, 397–401.

(58) (a) Stiefel, E. I. *Prog. Inorg. Chem.* **1977**, *22*, 1–223 and references therein. (b) Griffith, W. P. *Coord. Chem. Rev.* **1970**, *5*, 459–517. (c) Scheidt, W. R.; Tsai, Chun-Che; Hoard, J. L. *J. Am. Chem. Soc.* **1971**, *93*, 3867–3872. Scheidt, W. R.; Collins, D. M.; Hoard, J. L. *Ibid.* **1971**, *93*, 3873–3877. Schröder, F. A. *Acta Crystallogr., Sect. B* **1975**, *B31*, 2294–2309.

(59) (a) Griffith, N. P.; Wickins, T. D. *J. Chem. Soc. A* **1968**, 400–404. (b) See ref 58a. (c) Mingos, D. M. P. *J. Organomet. Chem.* **1979**, *179*, C29–C33. (d) Burdett, J. K.; Albright, T. A. *Inorg. Chem.* **1979**, *18*, 2112–2120. (e) Tatsumi, K.; Hoffmann, R. *Ibid.* **1980**, *19*, 2656–2658.

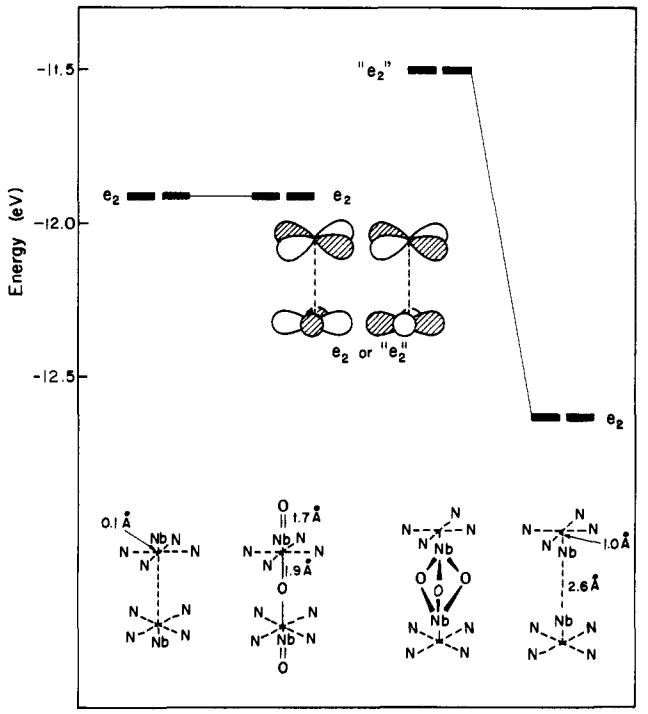


**Figure 8.** A comparison of the $e_2$ and the $e_2$-like energy levels of $(O{=}Nb{-}N_4)_2O$ and $(Nb{-}N_4)_2O_3$. For $(Nb{-}N_4)_2O_3$, the plane of the $O_3$ equilateral triangle bisects the line connecting the two Nb atoms which are located 1.3 Å above and below the center of the plane. The $e_2$ levels of $(Nb{-}N_4)_2$ fragments for $(O{=}Nb{-}N_4)_2O$ and $(Nb{-}N_4)_2O_3$ are given at the extreme left and the extreme right, respectively.

accompanies a greater stabilization of the $d_{yz}$ whose orbital lobes point between the N atoms of a porphyrin. The absence of a Nb d–O $p_\pi$ antibonding interaction in the $e_2$ level of the linear form leaves the $e_2$ untouched and provides a comfortable seat for the last two electrons. In structure **31**, the $e_2$ type orbitals are substantially destabilized due to an antibonding interaction between the $(Nb{-}N_4)_2$ $e_2$ level and "$O_3$" orbitals. The calculated energy difference between the $e_2$ of $(O{=}Nb{-}N_4)_2O$ and the "$e_2$" of $(Nb{-}N_4)$ amounts to 0.4 eV. We have attempted to estimate the "$e_2$" energy of the more realistic geometry **32** by moving the upper $(Nb{-}N_4)$ unit of **36** in the $+x'$ direction (+0.4 Å) and the lower unit in the $-x'$ direction (–0.4 Å), to see how the deformation affects the "$e_2$" level. The "$e_2$" level of **32** so approximated was calculated to lie at –11.2 eV, which is 0.3 eV higher than the "$e_2$" of **31**. The greater destabilization of the "$e_2$" indicates that the deformation enhances the Nb $d_{xy}$ (or $d_{x^2-y^2}$)–O p interactions and increases the energy gap between the $e_2$ of $(O{=}Nb{-}N_4)_2O$ and the "$e_2$" of $(Nb{-}N_4){-}O_3{-}(Nb{-}N_4)$. While the number cannot be relied on in a quantitative sense, the orbital energy difference must be a reason for the geometrical choice of $d^1$–$d^1$ porphyrin dimers of the $M_2O_3^{4+}$ type.

In the case of $d^2$–$d^2$ $(M{-}porphyrin)_2O_3$, the $e_2$–"$e_2$" energy gap has an even greater significance, simply because two additional electrons reside in the lowest $e_2$ d levels. Thus $d^2$–$d^2$ $(M{-}porphyrin)_2O_3$ should have a linear O=M–O–M=O bond, M = Mn(V), Tc(V), or Re(V) or the like.

We have to note here that although the linear structure of a $d^1$–$d^1$ $M_2O_3^{4+}$ unit minimizes the M $d_\pi$–O $p_\pi$ $\pi^*$ antibonding interaction, it also involves less $\pi$-bonding interaction than any other structure. Thus the geometrical choice may be a result of a balance between the two opposing factors. In $d^1$–$d^1$ $(ML_4)_2O_3$ complexes, the observed geometry is mostly **37** or **38** rather than **39**.[60] The linear O=M–O–M=O spine has been found only

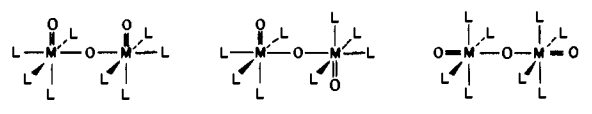

**37** **38** **39**

**Table I.** Parameters Used in the Extended Hückel Calculations

| orbital | $H_{ii}$, eV | exponents[a] $\zeta_1$ | $\zeta_2$ |
|---|---|---|---|
| Fe 4s | −8.39 | 1.90 | |
| 4p | −4.74 | 1.90 | |
| 3d | −11.46 | 5.35 (0.5366) | 1.80 (0.6678) |
| Nb 5s | −10.95 | 1.89 | |
| 5p | −7.59 | 1.85 | |
| 4d | −13.23 | 4.08 (0.6401) | 1.64 (0.5516) |
| Ru 5s | −7.73 | 2.08 | |
| 5p | −4.44 | 2.04 | |
| 4d | −11.23 | 5.378 (0.5340) | 2.303 (0.6365) |
| H 1s | −13.60 | 1.30 | |
| C 2s | −21.40 | 1.625 | |
| 2p | −11.40 | 1.625 | |
| N 2s | −26.00 | 1.950 | |
| 2p | −13.40 | 1.950 | |
| O 2s | −32.30 | 2.275 | |
| 2p | −14.80 | 2.275 | |

[a] The metal d functions are of a double-$\zeta$ type. The numbers in parentheses are the coefficients of the corresponding Slater orbitals.

for $d^1$–$d^1$ $(Mo{-}TPP)_2O_3$ and $(M{-}OEP)_2O_3$, M = Mo and W, and for $d^2$–$d^2$ $M_2O_3$ and $M_3O_4$ units such as $Re_2O_3(dtc)_2$[31b] and $[Re_3O_4(acac_2en)_3]^+$.[62] In geometries **37** and **38**, the out-of-phase combination of *xy* orbitals is left free of M–O $\pi$ interactions, as are the *yz* orbital combinations of **39**, while the in-phase pair of *xy* orbitals gets involved in M–O–M three-center $\pi$ bonding. Thus **37** and **38** are preferred to **39**, owing to the optimal M–O $\pi$ interactions.

Then why does $(Mo{-}TPP)_2O_3$ not choose **37** or **38**, the latter of which may be related to structure **32** of $(Nb{-}TPP)_2O_3$? **37** is excluded because two porphyrin rings come in contact with each other. When two porphyrins replace eight ligands L of **38**, the lowest out-of-phase combination of *xy* orbitals is tilted in order to ease a primary repulsive interaction with porphyrin orbitals. This is drawn schematically in **40**. The porphyrins are eclipsed

**40** **41**

to each other, which allows us to make a direct comparison between the lowest level in **38** and the orbital of **40**. As a result of the tilting, the lowest d orbital combination is no longer free from M–O $\pi^*$ interaction. Thus the two d electrons of $d^1$–$d^1$ $(Mo{-}TPP)_2O_3$ prefer residing in the *yz* combinations of **39** to sitting in **40**. The change of conformation from an eclipsed one to a staggered one, **41**, does not spoil the above argument.

This is the first paper of a series discussing the electronic structure of atypical metalloporphyrins. The second paper will address the structure of porphyrins coordinated to two $ML_n$ groups, porphyrin carbene complexes, oxoiron porphyrins, and acetylene addition to Co(TMTAA).

**Acknowledgment.** We are grateful to C. K. Chang, K. M. Kadish, G. N. La Mar, D. Mansuy, and W. R. Scheidt for in-

(60) An excellent discussion on this problem is available at pp 74–82 of ref 58a.
(61) Buchler, J. W.; Rohbock, K. *Inorg. Nucl. Chem. Lett.* **1972**, *8*, 1073–1076.
(62) Carrondo, M. A. A. F. de C. T.; Middleton, A. R.; Skapski, A. C.; West, A. P.; Wilkinson, G. *Inorg. Chim. Acta* **1980**, *44*, L7–L8.
(63) Lecomte, C.; Protas, J. *J. Chem. Soc., Chem. Commun.* **1976**, 434–435.
(64) Richardson, J. W.; Nieuwpoort, W. C.; Powell, R. R.; Edgell, W. F. *J. Chem. Phys.* **1962**, *36*, 1057–1061.
(65) See, for example: Summerville, R. H.; Hoffmann, R. *J. Am. Chem. Soc.* **1976**, *98*, 7240–7254. Albright, T. A.; Hofmann, P.; Hoffmann, R. *Ibid.* **1977**, *99* 7546–7557.
(66) Basch, H.; Gray, H. B. *Theor. Chim. Acta* **1966**, *4*, 367–376.

forming us of their experimental results prior to publication. Preliminary studies of porphyrin dimers of the $(N_4M)_2X$ type were carried out in our group 3 years ago by M.-H. Whangbo. We thank E. Stolz for the typing, J. Jorgensen for the drawings, and the National Science Foundation for its support of this work through Research Grants CHE 7828048 and DMR-7681083 to the Materials Science Center at Cornell University.

## Appendix

The Coulomb integrals for iron, niobium, and ruthenium were obtained from charge-iterative calculations on planar $Fe-(NH_2)_4^{2-}$. $(H_2N)_4-Nb=O(OOCH)^{2-}$, and $Ru(NH_3)_6^{2+}$. The geometrical parameters of the Nb=O(OOCH) portion were taken from the structure of (TPP)Nb=O($OOCCH_3$).[63] The Ru—N and N—H distances were assumed to be 2.15 and 1.03 Å in the octahedral molecule $Ru(NH_3)_6^{2+}$. Orbital exponents for the iron 3d functions are those given by Richardson et al.,[64] while those for the 4s and 4p orbitals are taken from previous work.[65] The Basch and Gray orbitals are used for the 4d, 5s, and 5p functions of niobium and ruthenium.[66] These extended Hückel parameters are listed in Table I, together with those for hydrogen, carbon, nitrogen, and oxygen atoms.

# Specific Sequestering Agents for the Actinides. 6. Synthetic and Structural Chemistry of Tetrakis(*N*-alkylalkanehydroxamato)thorium(IV) Complexes[1]

**William L. Smith and Kenneth N. Raymond***

*Contribution from the Department of Chemistry and Materials and Molecular Research Division, Lawrence Berkeley Laboratory, University of California, Berkeley, California 94720.*
*Received June 2, 1980*

**Abstract:** Hydroxamate complexes of the actinides have been investigated as structural archetypes in the design of actinide-specific sequestering agents. The complexes $Th[(CH_3)_2CHN(O)O(O)R]_4$ have been prepared, from aqueous solutions of Th(IV) and the corresponding hydroxamic acid, for $R = C(CH_3)_3$ or $CH_2C(CH_3)_3$ (compounds **1** and **2**, respectively). Both complexes **1** and **2** are hydrocarbon soluble and remarkably volatile, subliming near 100 °C ($10^{-3}$ torr). They are fluxional and rapidly exchange hydroxamate ligands in $CHCl_3$ solution. The uranium(IV) analogue of **1** was also prepared, but the uranium(IV) hydroxamates undergo an internal redox reaction that involves oxygen atom transfer from the ligand to the metal to give a bis(hydroxamato)uranyl complex and the amide of one hydroxamate ligand. The physical properties of the thorium hydroxamate complexes seem to be due to their hydrocarbon substituents, and the different steric constraints imposed by the C-substituent *tert*-butyl and neopentyl groups of **1** and **2**, respectively, give rise to dramatically different coordinate geometries. The *tert*-butyl groups of **1** dominate the stereochemistry of the complex by assuming a tetrahedral disposition around the metal. The coordination polyhedron of **1**, which has $\bar{4}$ ($S_4$) crystallographic symmetry, is nearly cubic. The localization of charge on the nitrogen oxygen of the hydroxamate group makes this ligand unsymmetrical, and this gives rise to a 0.14-Å difference in $R(Th-O_N)$ [2.357 (3) Å] and $R(Th-O_C)$ [2.492 (3) Å]. The sterically less constrained neopentyl derivative **2** shows a more typical eight-coordinate geomerty—the $D_{2d}$ trigonal-faced (*mmmm*) dodecahedron. Although there is no crystallographically imposed symmetry for **2**, the polyhedron is close to the ideal dodecahedron. The average $R(Th-O_N)$ [2.36 (1) Å] is again shorter than $R(Th-O_C)$ [2.46 (2) Å]. There is apparently no sorting of sites by ligand charge, since the $O_N$ and $O_C$ atoms are equally distributed between the A and B sites of the dodecahedron. Detailed analysis of the geometries of **1** and **2** are carried out in terms of their shape parameters and explicitly compared to related eight-coordinate complexes. Both compounds **1** and **2** are colorless. Crystals of **1** conform to space group $I4_1/a$ with $a = 17.338$ (4) Å and $c = 12.706$ (4) Å. For 4 formula units per cell the calculated density $d_{calcd}$ is 1.50 g cm$^{-3}$ and $d_{obsd}$ is 1.50 (1) g cm$^{-3}$. Crystals of **2** conform to space group $P\bar{1}$ with $a = 9.777$ (2) Å, $b = 14.633$ (2) Å, $c = 18.515$ (1) Å, $\alpha = 74.061_0$ (8), $\beta = 88.41$ (1)°, and $\gamma = 74.71$ (2)°. For 2 formula units per cell $d_{calcd} = 1.30$ g cm$^{-3}$ and $d_{obsd} = 1.19$ g cm$^{-3}$. Full-matrix least-squares refinement of both structures using all averaged, independent data with $F^2 > 3\sigma(F)^2$ gave for **1** with 1798 data and 117 variables $R = 0.027$ and $R_w = 0.032$ and for **2** with 6978 data and 467 variables $R = 0.034$, $R_w = 0.042$.

A biomimetic approach to the design of tetravalent actinide-specific sequestering agents modeled after bacterial iron-transport agents has suggested the incorporation of catechol or hydroxamic acid ligating groups in an octadentate macrochelate.[1,2] The complexes formed by actinide(IV) ions and these ligands, in which the steric constraints of a macrochelate are absent, serve as structural archetypes for designing the optimum actinide(IV) macrochelate. The actinide(IV) catecholates have been observed[3] to have coordination polyhedra very close to the idealized trigonal-faced dodecahedron in which the *m* edges are spanned by the ligands. While hydroxamic acids have been used in quantitative analysis and solvent extraction of actinides,[4] the complexes formed have not been structurally characterized. In order to characterize fully the formulation and coordination geometry of these compounds, we have determined the structures of tetrakis(*N*-isopropyl-3,3-dimethylbutanehydroxamato)- and tetrakis(*N*-isopropyl-2,2-dimethylpropanehydroxamato)thorium(IV) (Figure 1) by single-crystal X-ray diffraction.

## Experimental Section

The hydroxamic acids were synthesized as described elsewhere.[5] Anhydrous $UCl_4$ was purchased from ROC/RIC and $ThCl_4 \cdot 8H_2O$ was obtained from City Chemical Co. Reactions using U(IV) were performed under dry argon on a vacuum line using degassed solvents. Solutions of U(IV) were manipulated by using Schlenk techniques, and solids were handled in a Dri-Lab HE-43 glovebox under dry argon.

(1) Previous paper in this series: (a) Weitl, F. L.; Raymond, K. N.; Durbin, P. W. *J. Med. Chem.*, **1981**, *24*, 203-206. For recent reviews see: (b) Smith, W. L.; Raymond, K. N. *Struct. Bonding (Berlin)* **1981**, *43*, 159-186. (c) Raymond, K. N.; Smith, W. L.; Weitl, F. L.; Durbin, P. W.; Jones, E. S.; Abu-Dari, K.; Sofen, S. R.; Cooper, S. R. *ACS Symp. Ser.* **1980**, *131*, 143-172. (d) Raymond, K. N.; Harris, W. R.; Carrano, C. J.; Weitl, F. L. *Ibid.* **1980**, *140*, 313-332.

(2) Weitl, F. L.; Raymond, K. N.; Smith, W. L.; Howard, T. R. *J. Am. Chem. Soc.* **1978**, *100*, 1170-2.

(3) (a) Sofen, S. R.; Cooper, S. R.; Raymond, K. N. *Inorg. Chem.* **1979**, *18*, 1611-6. (b) Sofen, S. R.; Abu-Dari, K.; Freyberg, D. P.; Raymond, K. N. *J. Am. Chem. Soc.* **1978**, *100*, 7882-7.

(4) Smith, W. L.; Raymond, K. N. *J. Inorg. Nucl. Chem.* **1979**, *41*, 1431-6.

(5) Smith, W. L.; Raymond, K. N., submitted for publication.

0002-7863/81/1503-3341$01.25/0 